NASA TECHNICAL NOTE

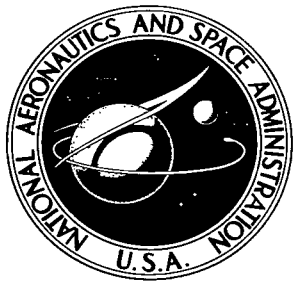

NASA TN D-8133

NASA TN D-8133

LOW-SPEED WIND-TUNNEL INVESTIGATION OF SPAN LOAD ALTERATION, FORWARD-LOCATED SPOILERS, AND SPLINES AS TRAILING-VORTEX-HAZARD ALLEVIATION DEVICES ON A TRANSPORT AIRCRAFT MODEL

Delwin R. Croom and R. Earl Dunham, Jr.

Langley Research Center
Hampton, Va. 23665

NATIONAL AERONAUTICS AND SPACE ADMINISTRATION • WASHINGTON, D. C. • DECEMBER 1975

1. Report No.	2. Government Accession No.	3. Recipient's Catalog No.
NASA TN D-8133		

4. Title and Subtitle
LOW-SPEED WIND-TUNNEL INVESTIGATION OF SPAN LOAD ALTERATION, FORWARD-LOCATED SPOILERS, AND SPLINES AS TRAILING-VORTEX-HAZARD ALLEVIATION DEVICES ON A TRANSPORT AIRCRAFT MODEL

5. Report Date: December 1975

6. Performing Organization Code:

7. Author(s)
Delwin R. Croom and R. Earl Dunham, Jr.

8. Performing Organization Report No.: L-10568

10. Work Unit No.: 514-52-01-03

9. Performing Organization Name and Address
NASA Langley Research Center
Hampton, Va. 23665

11. Contract or Grant No.:

13. Type of Report and Period Covered: Technical Note

12. Sponsoring Agency Name and Address
National Aeronautics and Space Administration
Washington, D.C. 20546

14. Sponsoring Agency Code:

15. Supplementary Notes

16. Abstract

An investigation was made in the Langley V/STOL tunnel to determine the effectiveness of a forward-located spoiler, a spline, and a span load alteration due to a flap configuration change as trailing-vortex-hazard alleviation methods. For the transport aircraft model in the normal approach configuration, the results indicate that either a forward-located spoiler or a spline is effective in reducing the trailing-vortex hazard. The results also indicate that large changes in span loading, due to retraction of the outboard flap, may be an effective method of reducing the trailing-vortex hazard.

17. Key Words (Suggested by Author(s))
Vortex alleviation
Trailing-vortex hazard

18. Distribution Statement
Unclassified – Unlimited

Subject Category 02

19. Security Classif. (of this report)	20. Security Classif. (of this page)	21. No. of Pages	22. Price*
Unclassified	Unclassified	46	$3.75

*For sale by the National Technical Information Service, Springfield, Virginia 22161

LOW-SPEED WIND-TUNNEL INVESTIGATION OF SPAN LOAD ALTERATION, FORWARD-LOCATED SPOILERS, AND SPLINES AS TRAILING-VORTEX-HAZARD ALLEVIATION DEVICES ON A TRANSPORT AIRCRAFT MODEL

Delwin R. Croom and R. Earl Dunham, Jr.
Langley Research Center

SUMMARY

An investigation was made in the Langley V/STOL tunnel to determine, by the trailing wing sensor technique, the effectiveness of a large change in span load distribution, a forward-mounted spoiler, and a trailing drag device (spline) as trailing-vortex-hazard alleviation devices on a swept-wing transport aircraft model.

The induced rolling-moment coefficient on the trailing models at a given lift coefficient of the generating model was generally larger for the large trailing wing model than for the small trailing wing model, and the variation of trailing wing rolling-moment coefficient with lift coefficient of the generating model was generally greater for the large trailing model than for the small trailing model.

The induced rolling-moment coefficient on both trailing wing models was reduced when the horizontal-tail incidence angle of the generating model was decreased to a point where a download on the horizontal tail was produced.

At scale downstream distances behind the generating model of less than about 16 spans, the induced trailing wing rolling-moment coefficient was larger for the flap configuration with only the inboard flap deflected to 30° than for the flap configuration with both inboard and outboard flaps deflected to 30°. At scale downstream distances greater than 16 spans, the induced trailing wing rolling-moment coefficients were smaller for the configuration with only the inboard flaps deflected than those for the configuration with inboard and outboard flaps deflected. These results indicate that large changes in span loading due to retraction of the outboard flap may be an effective method of reducing the trailing-vortex hazard.

For the transport aircraft model in the normal approach configuration (inboard and outboard flaps deflected to 30°) either a forward-located midspan spoiler or a spline reduces the induced rolling-moment coefficient on the small trailing model by

about 35 to 40 percent throughout the downstream distances investigated. The reduction in induced rolling-moment coefficient on the large trailing model was much less (about 15 to 25 percent).

INTRODUCTION

The strong vortex wakes generated by large transport aircraft are a potential hazard to smaller aircraft. The National Aeronautics and Space Administration is involved in a program of model tests, flight tests, and theoretical studies to determine the feasibility of reducing this hazard by aerodynamic means.

Previous work (ref. 1) has shown that the magnitude of the vortex-wake hazard is greatly influenced by the direction of the flight of the aircraft which is penetrating the trailing vortices. As discussed in reference 1, a cross-track penetration at right angles to the trailing vortices tends to cause pitching and vertical motion and to produce vertical loads on the penetrating airplane in a manner similar to that of a gust encounter. Also, an along-track penetration, parallel to and between the wing-tip vortices, can occur in both the take-off climbout and the landing approach and may cause settling or, at least, may reduce the rate of climb of the penetrating aircraft. However, an along-track penetration through the vortex center is considered to be the most hazardous encounter since such penetration would induce a rolling motion to the penetrating aircraft that could result in an upset.

One approach in assessing the trailing-vortex hazard is to determine the velocity profile of the vortex and, by integrating the velocity profile over the span of the penetrating aircraft, the induced rolling moment can be inferred. Detailed measurements of the velocity profile through the trailing vortex have been obtained by the use of attitude sensor vanes and total-pressure probes (ref. 2), yawheads (ref. 3), tuft grids (ref. 4), vortex meters (ref. 5), and hot-wire anemometers (ref. 6). Another approach in assessing the trailing-vortex hazard is to simulate an airplane flying in the trailing vortex and to make direct measurements of the individual rolling moments.

The results of a recent wind-tunnel investigation which used the direct-measurement technique (ref. 7) has indicated that the trailing-vortex hazard behind an unswept wing model can be attenuated by use of either a forward-mounted spoiler or a spline. The flight test results of reference 8 also indicated that a spline device could be used to attenuate the vortex system of an unswept wing aircraft.

The purpose of the present investigation is to determine the effectiveness of a forward-located spoiler, a spline, and a span load alteration due to a flap configuration change as trailing-vortex-hazard alleviation methods.

The technique used in the present investigation in assessing the trailing-vortex hazard is to simulate an airplane flying the trailing vortex and to make direct measurements of the rolling moments induced on the trailing model by the vortex generated by the forward model.

SYMBOLS

All data are referenced to the wind axes. The pitching-moment coefficients are referenced to the quarter-chord of the wing mean aerodynamic chord.

b	wing span, m
C_D	drag coefficient, $\frac{\text{Drag}}{qS_W}$
C_L	lift coefficient, $\frac{\text{Lift}}{qS_W}$
$C_{l,TW}$	trailing wing rolling-moment coefficient, $\frac{\text{Trailing wing rolling moment}}{qS_{TW}b_{TW}}$
C_m	pitching-moment coefficient, $\frac{\text{Pitching moment}}{qS_W\bar{c}_W}$
c	wing chord, m
$\bar{c}$	wing mean aerodynamic chord, m
i_t	horizontal-tail incidence, referred to fuselage reference line (positive direction trailing edge down), deg
l	longitudinal distance in tunnel diffuser, m
q	dynamic pressure, Pa
S	wing area, m^2
X',Y',Z'	system of axes originating at left wing tip of transport aircraft model (see fig. 1)
x',y',z'	longitudinal, lateral, and vertical dimensions measured from trailing edge of wing tip of transport aircraft model, m

$\Delta y', \Delta z'$ incremental dimensions along Y'- and Z'-axes, m

α angle of attack of fuselage reference line, deg (wing incidence is 2° relative to fuselage reference line)

ϕ local streamline angle in tunnel diffuser relative to tunnel center line, deg

$\delta_{f,i}$ nominal deflection of inboard segment of flap, deg

$\delta_{f,o}$ nominal deflection of outboard segment of flap, deg

Subscripts:

W transport aircraft model

TW trailing wing model

max maximum

MODELS AND APPARATUS

A three-view sketch and principal geometric characteristics of the 0.03-scale model of a jumbo-jet transport aircraft are shown in figure 1. Figures 2 and 3 are photographs of the model in the Langley V/STOL tunnel. The fuselage, empennage, wings, trailing-edge flaps, and leading-edge devices of this model were constructed by using a mold made from the model discussed in reference 9. The trailing-edge flaps used on the model of reference 9 were appended to the complete wing and, therefore, were not representative of flap arrangements used on actual aircraft. For the model used in the present investigation, the trailing edge of the wing was altered and the triple-slotted trailing-edge flaps were relocated to more nearly represent a flap arrangement that would be used on an actual aircraft. The all-movable horizontal tail was mounted on a shaft through a friction block which allowed the tail incidence to be set at any desired angle.

Photographs and dimensions of the spline and the forward-located midspan spoiler installed on the transport aircraft model are presented in figures 4 and 5, respectively.

Photographs and dimensions of the two unswept trailing wing models installed on the traverse mechanism are presented in figure 6. The large trailing model has a span and aspect ratio typical of a medium-size transport aircraft, and the small trailing model has a span and aspect ratio typical of a small-size transport aircraft.

The Langley V/STOL tunnel has a test-section height of 4.42 m, a width of 6.63 m, and a length of 15.24 m. The transport aircraft model was sting supported on a six-component, strain-gage balance system which measured the forces and moments. The angle of attack was determined from an accelerometer mounted in the fuselage. The trailing models were mounted on a single-component, strain-gage roll balance, which was attached to a traverse mechanism capable of moving the model both laterally and vertically (see fig. 6). The lateral and vertical positions of the trailing model were measured by outputs from digital encoders. This entire traverse mechanism could be mounted on the tunnel floor at various tunnel longitudinal positions downstream of the transport aircraft model.

TESTS AND CORRECTIONS

Transport Aircraft Model

All tests were run at a free-stream dynamic pressure in the tunnel test section of 430.9 Pa which corresponds to a velocity of 27.4 m/sec. The Reynolds number for the tests was approximately 4.7×10^5 based on the wing mean aerodynamic chord. Transition strips approximately 0.30 cm wide of No. 60 abrasive grit were placed 2.54 cm back of the leading edge of the wing, whereas natural transition was used elsewhere. The basic longitudinal aerodynamic characteristics were obtained through an angle-of-attack range of approximately -4° to 24°. Each configuration was tested at several tail incidence angles and with the horizontal tail off. All the tests were made with leading-edge devices extended.

Blockage corrections were applied to the data by the method of reference 10. Jet-boundary corrections to the angle of attack and to the drag were applied in accordance with reference 11.

Trailing Wing Models

Each trailing wing model and its associated roll-balance system was used as a sensor to measure the induced rolling moment caused by the vortex flow downstream of the transport aircraft model. No transition grit was applied to the trailing models. The trailing model was positioned at a given distance downstream of the transport aircraft model and the traverse mechanism was positioned laterally and vertically so that the trailing vortex was near the center of the mechanism. The trailing vortex was probed with the trailing models. A large number of trailing wing rolling-moment data points (usually from 50 to 100) were obtained from the lateral traverses at several vertical locations to insure good definition of the vortex wake. Additionally, certain test

conditions were repeated at selected intervals during the test period and the data were found to be repeatable throughout the test period.

Trailing wing rolling-moment measurements were made at downstream scale distances from about 7 to 27 spans behind the transport aircraft model. All the trailing wing rolling-moment data at distances downstream greater than about 7 spans were obtained with the trailing model positioned in the diffuser section of the V/STOL tunnel. These data were reduced to coefficient form based on the dynamic pressure at the trailing wing location. For these tests, the dynamic pressures at the 6.74, 13.48, 20.22, and 26.96 span locations were 430.9, 262.3, 142.9, and 82.5 Pa, respectively. The trailing wing location relative to the wing tip of the transport aircraft model has been corrected to account for the progressively larger tunnel cross-sectional area in the diffuser section. The corrections to the trailing wing location in the diffuser were made by assuming that the local streamline angles in the tunnel diffuser section are equal to the ratio of the distance from the tunnel center line to the local tunnel half-width or tunnel half-height multiplied by the diffuser half-angle. Corrections to the trailing model locations are as follows: $\Delta y'$ correction or $\Delta z'$ correction $= l \tan \phi$ where $\Delta y'$ correction and $\Delta z'$ correction are, respectively, the corrections to the measured lateral and vertical locations of the trailing model relative to the tip of the transport aircraft model, l is the longitudinal distance in the tunnel diffuser, and ϕ is the local streamline angle in the tunnel diffuser relative to the tunnel center line.

RESULTS AND DISCUSSION

Transport Aircraft Model

The longitudinal aerodynamic characteristics of the transport aircraft model with both the inboard and outboard sections of the trailing-edge triple-slotted flaps deflected 30° (hereafter referred to as flap configuration $30^{\circ}/30^{\circ}$) and with only the inboard section of the flap deflected 30° (hereafter referred to as flap configuration $30^{\circ}/0^{\circ}$) are presented in figures 7 and 8, respectively. It is assumed that configuration change from the complete flap system ($30^{\circ}/30^{\circ}$) to the deflection of the inboard flaps only ($30^{\circ}/0^{\circ}$) creates a large change in span load distribution. The span loadings for these tests were not measured. These data were obtained over a range of horizontal-tail incidence sufficient to trim the model throughout the range of lift coefficient and with the horizontal tail off so that the direction of load on the horizontal tail could be determined.

These data indicate that the transport aircraft model with either flap configuration exhibited pitch-up near stall. These data also indicate that the static margin $\partial C_m/\partial C_L$ is less for the model with flap configuration $30^{\circ}/0^{\circ}$ than for the model with flap configuration $30^{\circ}/30^{\circ}$ $\left(\partial C_m/\partial C_L = -0.10 \text{ compared with } \partial C_m/\partial C_L = -0.18\right)$. It can also be seen

by comparing the tail-off and tail-on data in figures 7 and 8 that at $C_L = 1.2$, a download on the horizontal tail is required to trim the model with flap configuration $30^o/30^o$, whereas essentially no load on the horizontal tail is required to trim the model with flap configuration $30^o/0^o$. Therefore the rotational direction of the trailing vortex from the horizontal tail of flap configuration $30^o/30^o$ should be counter to the rotational direction of the wing and flap vortex, whereas there should be essentially no definable vortex flow from the horizontal tail of flap configuration $30^o/0^o$ since the lift on the horizontal tail is essentially zero.

The effects of forward-located spoilers and splines on the longitudinal aerodynamic characteristics of the transport aircraft model with flap configuration $30^o/30^o$ and with flap configuration $30^o/0^o$ are presented in figures 9 and 10, respectively. These results indicate that the splines did not appreciably alter the lift characteristics of the transport aircraft model. They act essentially as a pure drag device since they add a constant increment of drag throughout the angle-of-attack range. These results also indicate that the forward-located spoiler acts not only to produce drag but also to modify the lift characteristics of the model by reducing both the lift-curve slope and the maximum lift coefficient. In addition, a change in the span load distribution due to the forward-located spoiler would be expected.

Trailing Wing Models

From the rolling-moment data obtained with the trailing wing model, contour plots of constant rolling-moment coefficient were constructed as shown in figure 11. From contour plots such as these, the maximum rolling-moment coefficient and the location of the trailing model relative to the wing of the transport aircraft model were determined.

The position of the trailing wing models relative to the wing tip of the transport aircraft model and the maximum rolling-moment coefficient $(C_{l,TW})_{max}$ induced on the trailing wing models by the vortex generated by the transport aircraft model with flap configurations $30^o/30^o$ and $30^o/0^o$ are presented as functions of trimmed lift coefficient in figures 12 and 13, as functions of horizontal-tail incidence in figures 14 and 15, and as functions of downstream distance behind the transport aircraft model in figures 16 and 17. The trailing wing rolling-moment data are summarized in figures 18 to 21.

It can be seen in figure 18 that the trailing wing rolling-moment coefficient was generally larger for the large trailing model than for the small trailing model. Also, the variation of trailing wing rolling-moment coefficient with lift coefficient was generally greater for the large trailing model than for the small trailing model. Although it is recognized that an aircraft generates many trailing vortices (from flaps, wing tips, horizontal tail, etc.), it was thought that beyond about 10 to 15 spans downstream, the aircraft wake would have the essential characteristics of a single, predominant pair of vortices.

Such a vortex system should create a larger rolling-moment coefficient on the small trailing wing model than on the large trailing wing model, and the small wing should be more sensitive to variations in lift coefficient changes. The unexpected results with the small trailing wing were thought to be attributed to a stalled flow region caused by a large vortex-induced local angle of attack and the low Reynolds number of the test. A cursory look at the flow conditions on the small trailing wing equipped with tufts did not indicate a stalled condition. Consequently, the unexpected magnitude and variation with lift coefficient for the small trailing wing remains unexplained but may be associated with the unknown interaction of the multiple vortices on the trailing wing models.

It can be seen in figure 19 that the variation of $(C_{l,TW})_{max}$ with horizontal-tail incidence for both trailing wings was larger behind the transport aircraft model with flap configuration $30^o/0^o$ than behind the transport aircraft model with flap configuration $30^o/30^o$. This may be due to the resulting increased interactions of the tail and flap vortex systems because of their closer spanwise proximity with flap configuration $30^o/0^o$ than with flap configuration $30^o/30^o$.

It can also be seen in figure 19 that the trailing wing rolling-moment coefficient for both trailing wing models was reduced when the horizontal-tail incidence angle was decreased sufficiently to cause a download on the horizontal tail ($i_t \leq +4^o$ for flap configuration $30^o/30^o$, and $i_t \leq +3^o$ for flap configuration $30^o/0^o$ as shown by horizontal-tail-off and horizontal-tail-on data in figs. 7 and 8, respectively). This download on the horizontal tail would result in a vortex being generated by the horizontal tail with opposite rotation to the vortex generated by the wing and flaps. The interaction between these two vortex systems may be the cause of the reduction in trailing wing rolling-moment coefficient seen in figure 19 as the tail incidence angle was reduced.

The data in figure 20 indicate that a large change in the span loading on the transport aircraft model, associated with the flap configuration $30^o/0^o$ as compared with flap configuration $30^o/30^o$, does alter the induced rolling moments on the trailing wing models. At downstream distances of less than about 16 spans, the trailing wing rolling-moment coefficients for flap configuration $30^o/0^o$ were somewhat higher than those for flap configuration $30^o/30^o$; however, at downstream distances greater than about 16 spans, a definite decrease in trailing wing rolling-moment coefficient was noted. The wind-tunnel tests indicate that span load alteration due to retraction of the outboard flaps may be an effective means of reducing the trailing-vortex hazard. Subsequent flight test reports in reference 12 have indicated trends for flap configuration $30^o/0^o$ similar to those obtained in these tests.

The effectiveness of the spoilers and of the splines in reducing $(C_{l,TW})_{max}$ for the two trailing wing models downstream of the transport aircraft model equipped with flap configuration $30^o/30^o$ or with flap configuration $30^o/0^o$ is shown in figure 21.

The induced rolling-moment coefficients on the large trailing model downstream of the transport aircraft model with flap configuration $30^{o}/30^{o}$ or with flap configuration $30^{o}/0^{o}$ (figs. 21(c) and 21(d)) are larger than those induced on the small trailing model (figs. 21(a) and 21(b)).

The induced rolling-moment coefficient on the small trailing wing model, generated by the transport aircraft model with flap configuration $30^{o}/30^{o}$, was reduced by about 35 to 40 percent when either the midspan spoiler or the spline was used as vortex attenuators. (See fig. 21(a).) It can be seen in figure 21(b) that the induced rolling-moment coefficient on the small trailing wing model generated by the transport aircraft model with flap configuration $30^{o}/0^{o}$ was reduced only by about 10 percent as a result of the midspan spoiler and that the spline appeared to become ineffective at a downstream distance of about 17 spans.

For flap configuration $30^{o}/30^{o}$ (fig. 21(c)), the midspan spoiler caused reductions in the induced rolling-moment coefficient on the large trailing model of about 10 percent at 6.7 spans downstream and about 20 percent at 26.96 spans downstream. The effectiveness of the spline was comparable with the effectiveness of the midspan spoiler over the downstream range of about 7 to about 14 spans; however, the spline became ineffective at about 20 spans downstream.

For flap configuration $30^{o}/0^{o}$ (fig. 21(d)), the induced rolling-moment coefficient on the large trailing model was not reduced as a result of the midspan spoiler at downstream distances less than about 10 spans; however, the midspan spoiler was effective at downstream distances greater than about 10 spans. At the 26.96-span location the induced rolling-moment coefficient was reduced by about 30 percent. The spline, on the other hand, caused a small reduction (of the order of 5 percent) in induced rolling-moment coefficient at distances from about 7 spans to about 12 spans downstream, and near the 17-span location the splines become ineffective. The data obtained at the 26.96-span location, however, indicated that the splines regained some effectiveness with a reduction of about 15 percent in induced rolling-moment coefficient. The effectiveness of the spline may have been larger had it been located nearer the outboard end of the flap for flap configuration $30^{o}/0^{o}$.

CONCLUDING REMARKS

Results have been presented of an investigation in the Langley V/STOL tunnel to determine, by the trailing wing sensor technique, the effectiveness of a large change in span load distribution, a forward-mounted spoiler, and a spline as trailing-vortex hazard-alleviation devices on a swept-wing transport aircraft model.

The induced trailing wing rolling-moment coefficient, at a lift coefficient of 1.2, was generally larger for the large trailing model than for the small trailing model. Also, the

variation of trailing wing rolling-moment coefficient with trimmed lift coefficient was generally greater for the large trailing model than for the small trailing model.

The rolling-moment coefficient for both trailing wing models was reduced when the horizontal-tail incidence angle of the transport aircraft model was decreased sufficiently to cause a download on the horizontal tail.

At downstream distances of less than about 16 spans, the rolling-moment coefficient induced on both trailing wing models by flap configuration $30^{\circ}/0^{\circ}$ was somewhat higher than those induced by flap configuration $30^{\circ}/30^{\circ}$; however, at downstream distances greater than about 16 spans, a definite decrease in trailing wing rolling-moment coefficient was noted. This would indicate that span load alteration due to retraction of the outboard flap may be an effective method of reducing the trailing-vortex hazard.

The induced rolling-moment coefficient on the small trailing wing, generated by the transport aircraft model with flap configuration $30^{\circ}/30^{\circ}$, was reduced by about 35 to 40 percent when either the midspan spoiler or the spline was used as vortex attenuators. Neither device was as effective in reducing the induced rolling-moment coefficient on the large trailing model, resulting in a reduction of the order of 15 to 25 percent.

Langley Research Center
National Aeronautics and Space Administration
Hampton, Va. 23665
December 3, 1975

REFERENCES

1. Wetmore, Joseph W.; and Reeder, John P.: Aircraft Vortex Wakes in Relation to Terminal Operations. NASA TN D-1777, 1963.

2. Kraft, Christopher C., Jr.: Flight Measurements of the Velocity Distribution and Persistence of the Trailing Vortices of an Airplane. NACA TN 3377, 1955.

3. Mason, W. H.; and Marchman, J. F., III: The Farfield Structure of Aircraft Wake Turbulence. AIAA Paper No. 72-40, Jan. 1972.

4. Scheiman, James; and Shivers, James P.: Exploratory Investigation of the Structure of the Tip Vortex of a Semispan Wing for Several Wing-Tip Modifications. NASA TN D-6101, 1971.

5. McCormick, Barnes W.; Tangler, James L.; and Sherrieb, Harold E.: Structure of Trailing Vortices. J. Aircraft, vol. 5, no. 3, May-June 1968, pp. 260-267.

6. Corsiglia, V. R.; Schwind, R. G.; and Chigier, N. A.: Rapid Scanning, Three-Dimensional, Hot-Wire Anemometer Surveys for Wing Tip Vortices in the Ames 40- by 80-Foot Wind Tunnel. AIAA Paper No. 73-681, July 1973.

7. Croom, Delwin R.: Low-Speed Wind-Tunnel Investigation of Forward-Located Spoilers and Trailing Splines as Trailing-Vortex Hazard-Alleviation Devices on an Aspect-Ratio-8 Wing Model. NASA TM X-3166, 1975.

8. Hastings, Earl C., Jr.; Patterson, James C., Jr.; Shanks, Robert E.; Champine, Robert A.; Copeland, W. Latham; and Young, Douglas C.: Development and Flight Tests of Vortex-Attenuating Splines. NASA TN D-8083, 1975.

9. Kirkman, Karl L.; Brown, Clinton E.; and Goodman, Alex: Evaluation of Effectiveness of Various Devices for Attenuation of Trailing Vortices Based on Model Tests in a Large Towing Basin. NASA CR-2202, 1973.

10. Herriot, John G.: Blockage Corrections for Three-Dimensional-Flow Closed-Throat Wind Tunnels, With Consideration of the Effect of Compressibility. NACA Rep. 995, 1950. (Supersedes NACA RM A7B28.)

11. Gillis, Clarence L.; Polhamus, Edward C.; and Gray, Joseph L., Jr.: Charts for Determining Jet-Boundary Corrections for Complete Models in 7- by 10-Foot Closed Rectangular Wind Tunnels. NACA WR L-123, 1945. (Formerly NACA ARR L5G31.)

12. Smith, Harriet J.: A Flight Test Investigation of the Rolling Moments Induced on a T-37B Airplane in the Wake of a B-747 Airplane. NASA TM X-56031, 1975.

Wing

Span, m	1.79
Mean aerodynamic chord, m	0.25
Root chord, m	0.497
Tip chord, m	0.121
Sweepback at quarter chord, deg	37.5
Area, m^2	0.460
Aspect ratio	6.96

Fuselage

Length, m	2.06

Horizontal tail

Span, m	0.664
Area, m^2	0.123
Aspect ratio	3.6

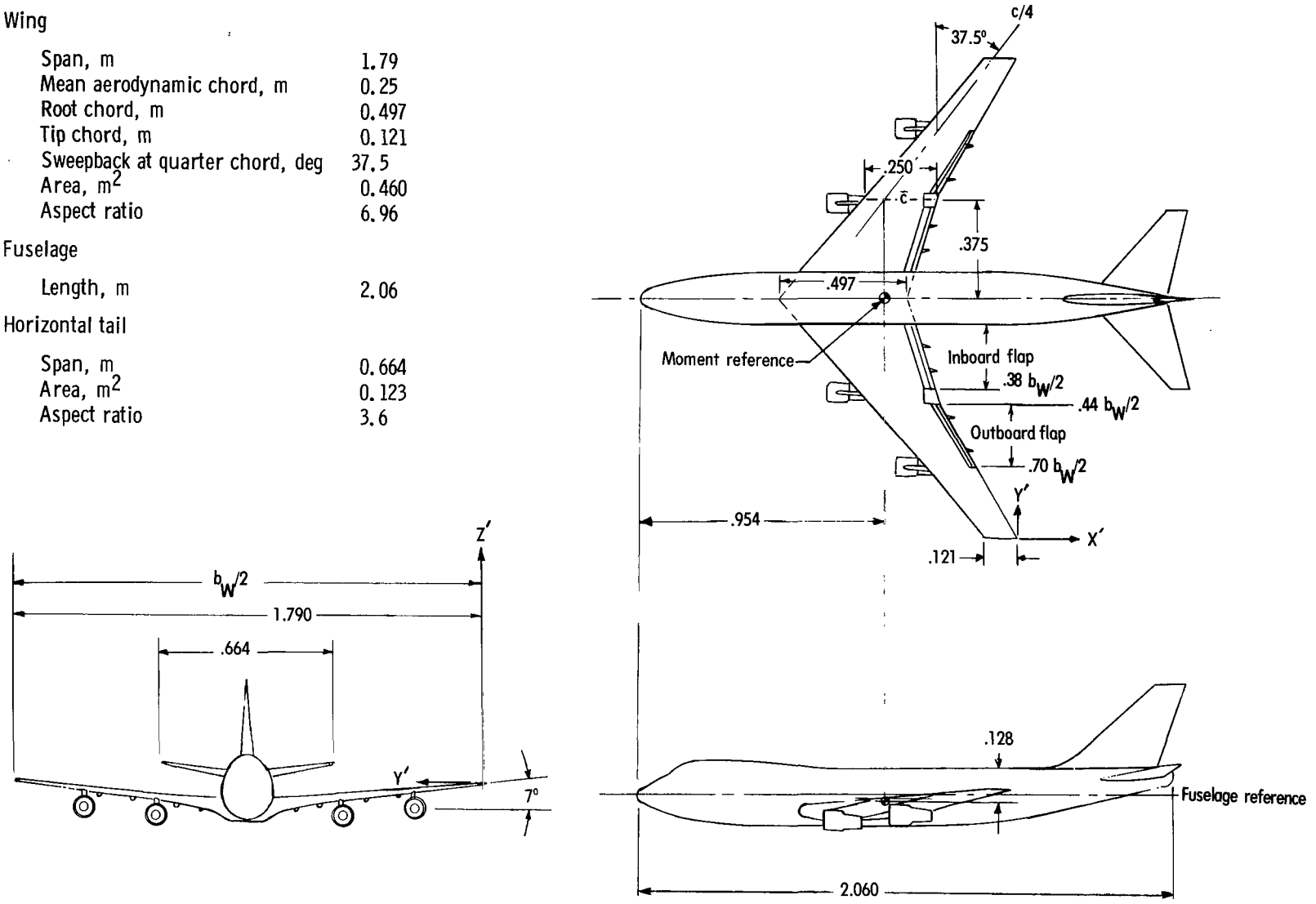

Figure 1.- Three-view sketch of transport aircraft model with flaps retracted. Linear dimensions are in meters.

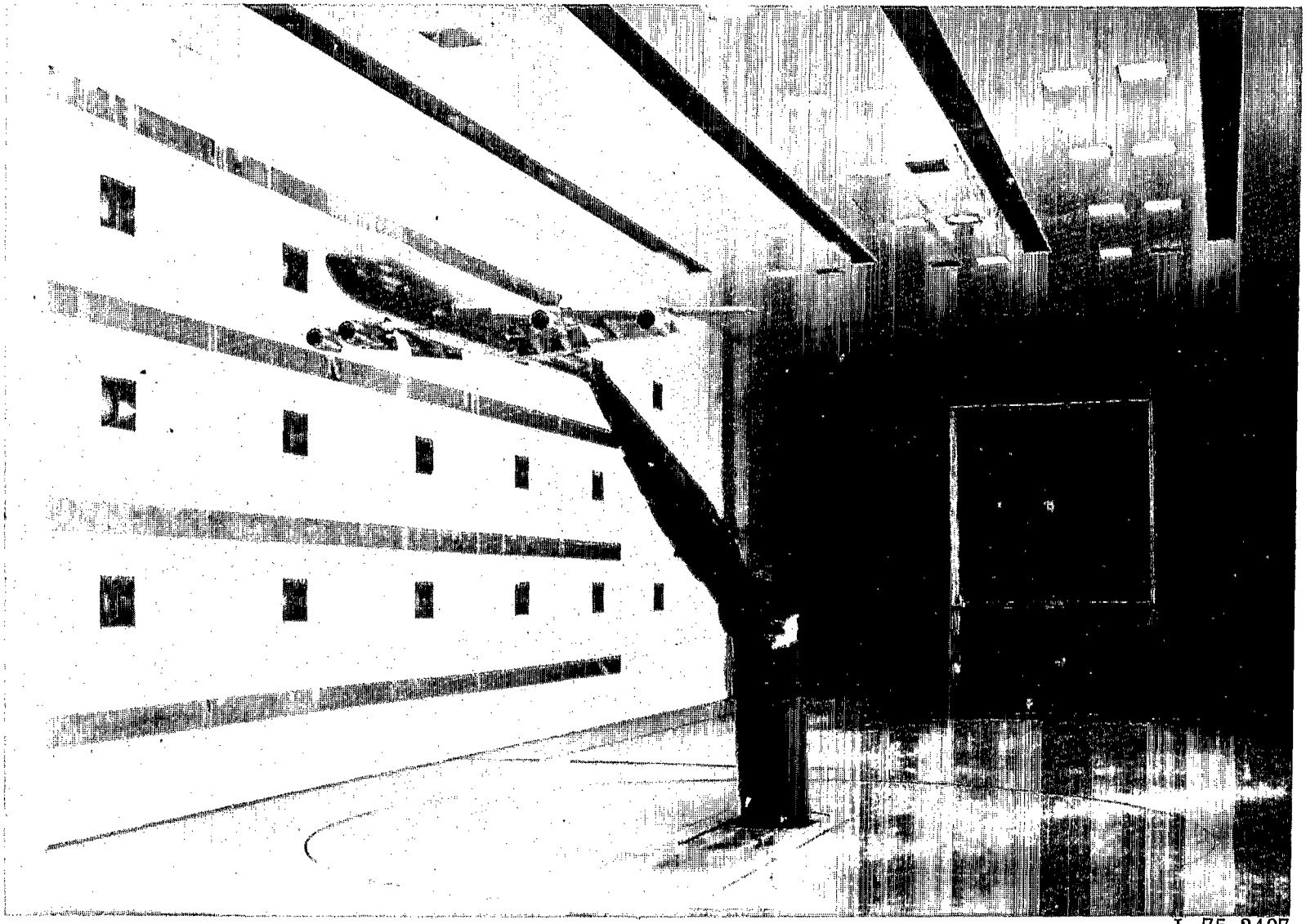

L-75-2407

Figure 2.- Photograph of transport aircraft model with flap configuration $30^{o}/30^{o}$.

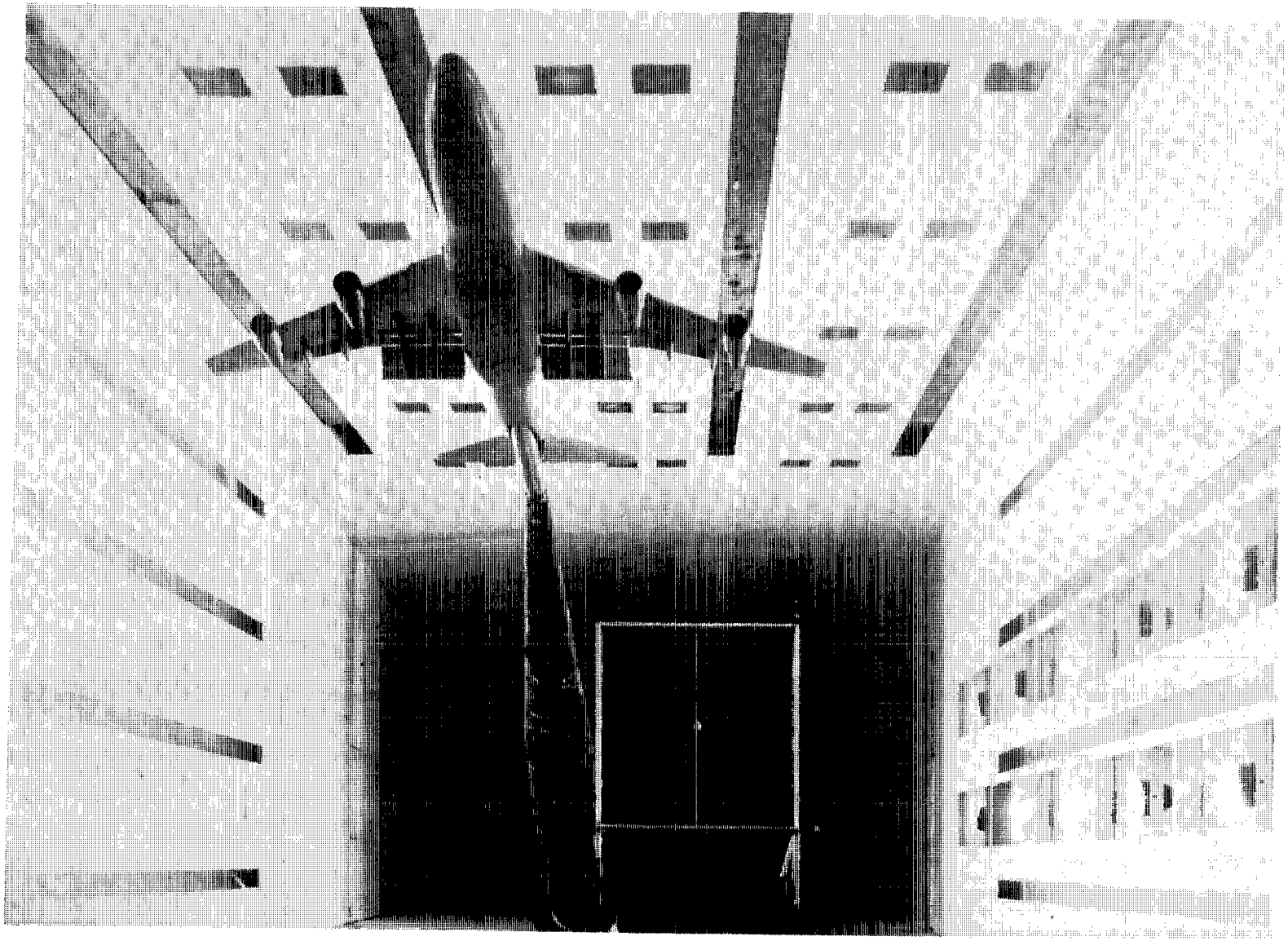

L-75-2406

Figure 3.- Photograph of transport aircraft model with flap configuration 30°/0°.

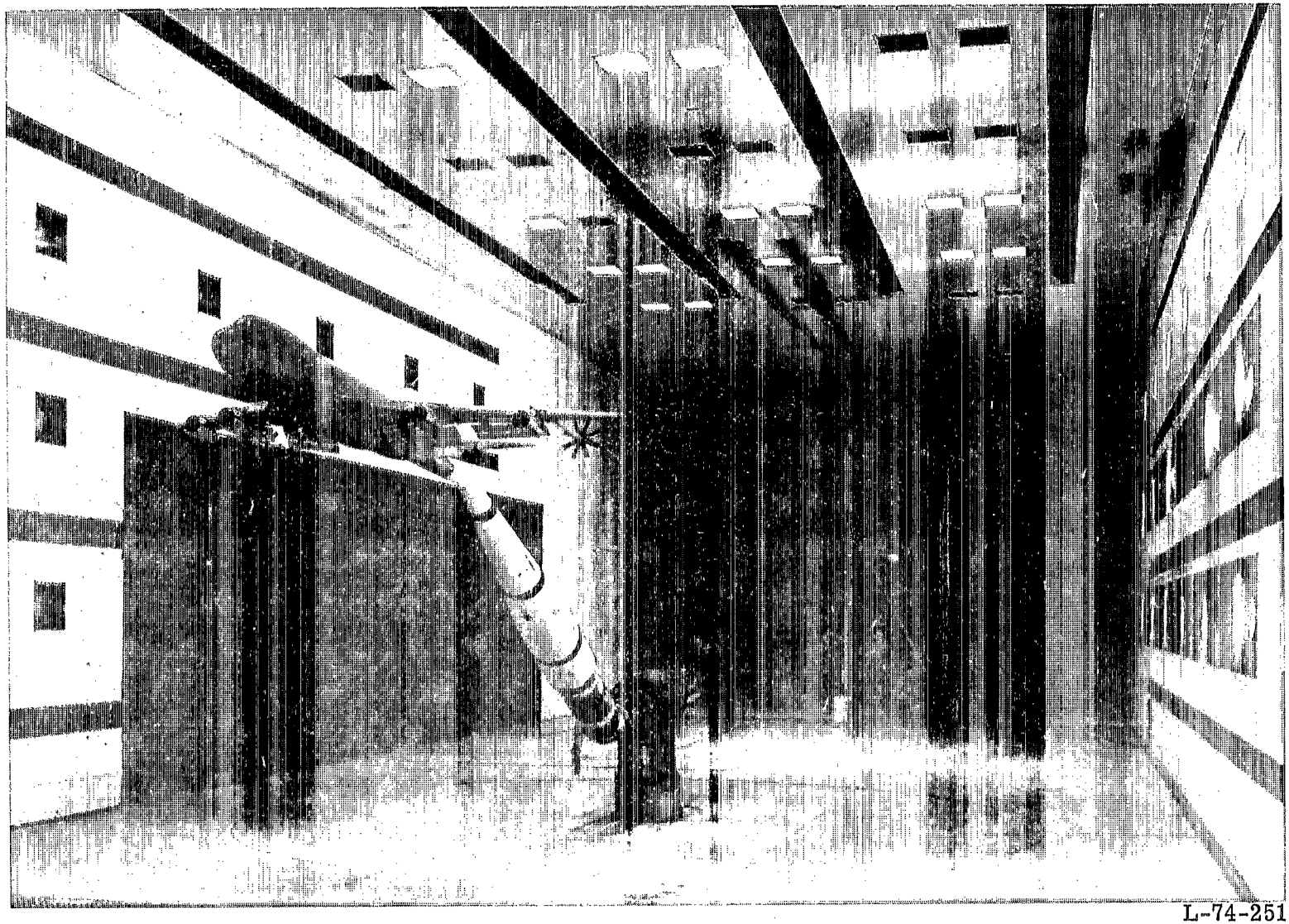

L-74-251

(a) Three-quarter front view of splines on transport aircraft model.

Figure 4.- Photograph, dimensions, and location of spline on transport aircraft model.

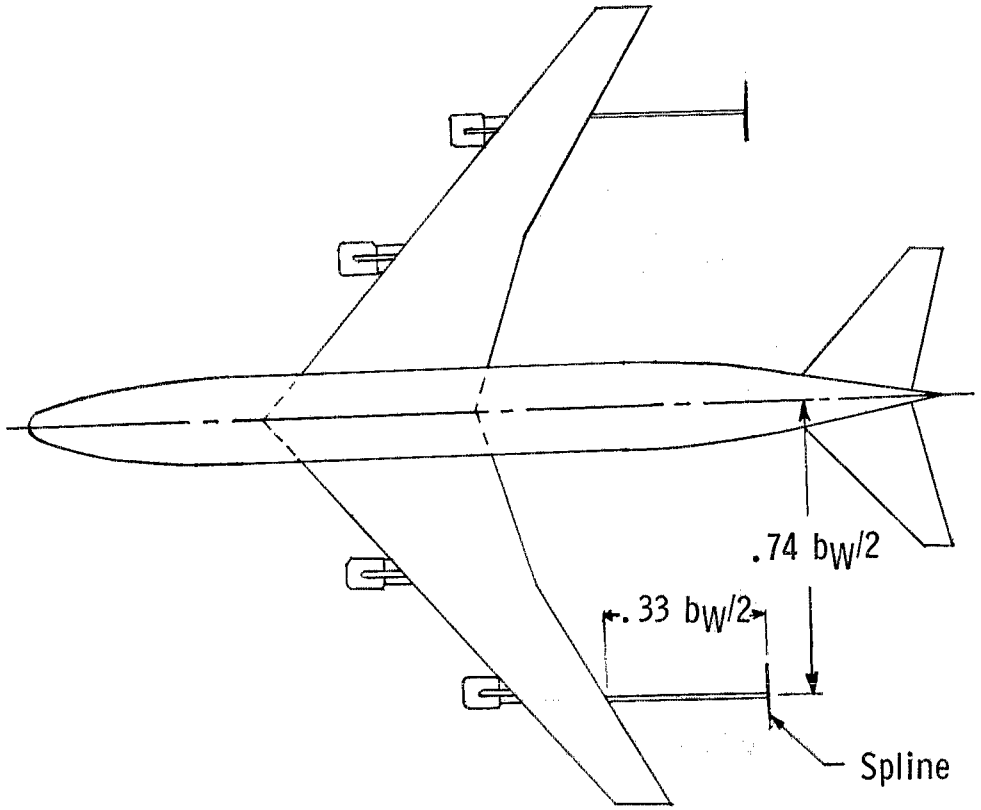

Spline location

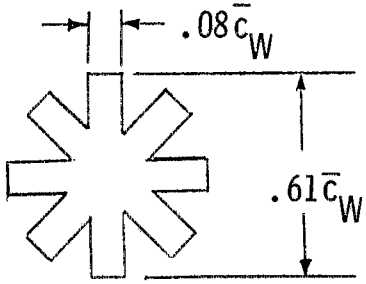

Spline planform

(b) Schematic of spline planform and spline location on transport aircraft model.

Figure 4.- Concluded.

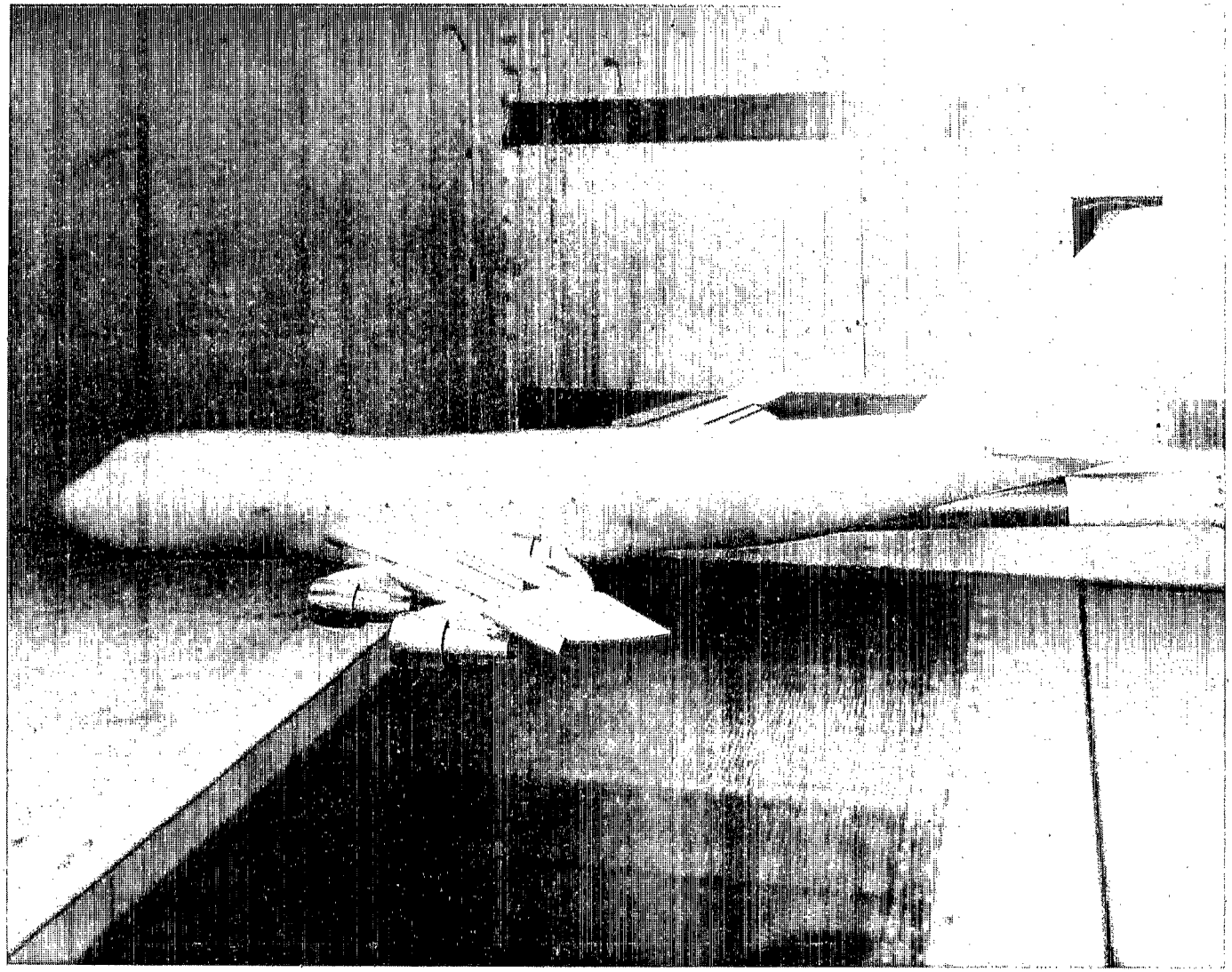

L-74-253

(a) Side view of midspan spoiler on transport aircraft model.

Figure 5.- Photograph, dimensions, and location of midspan spoiler on transport aircraft model.

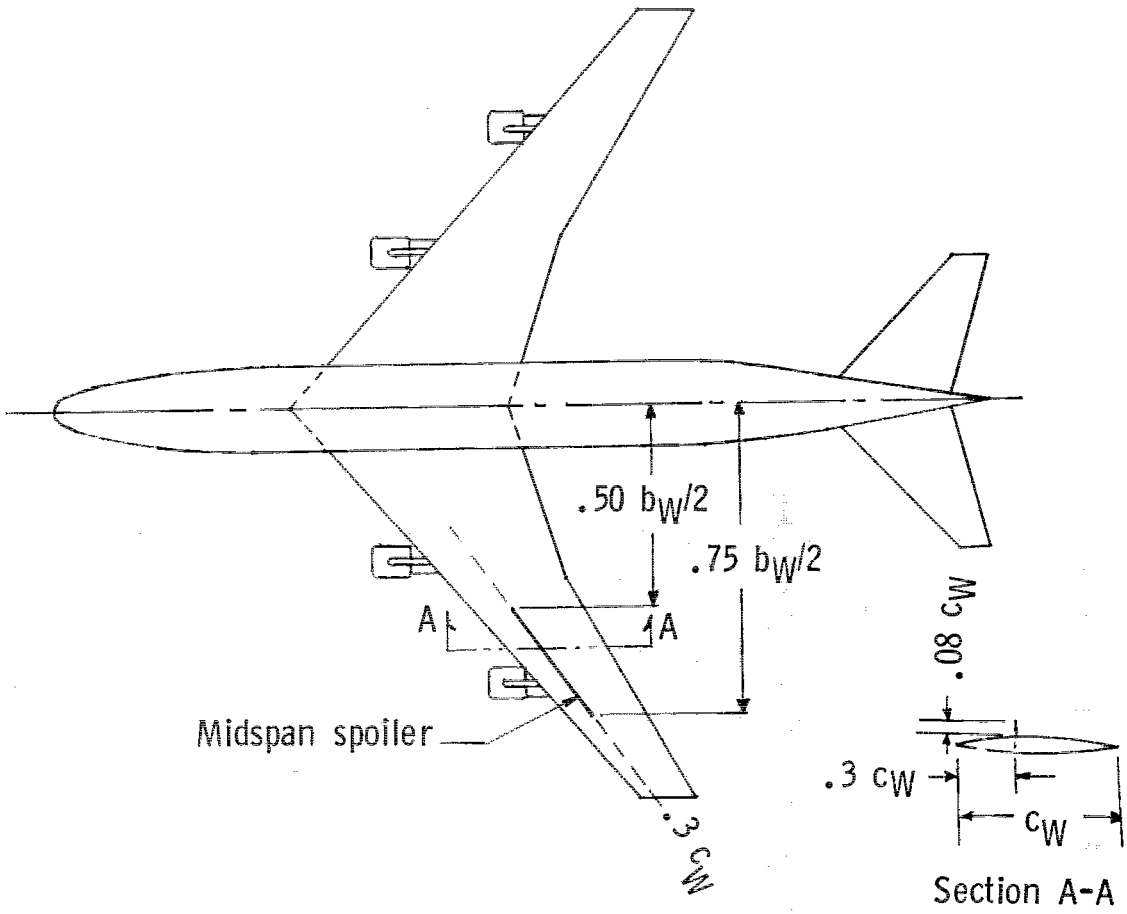

(b) Schematic showing midspan spoiler projection and location on transport aircraft model.

Figure 5.- Concluded.

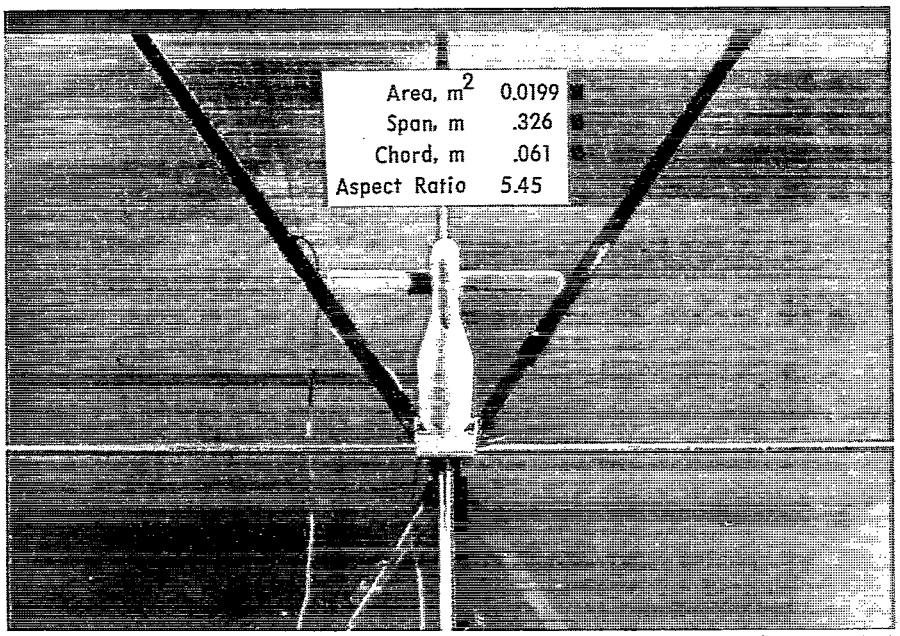

L-75-2411.1

(a) Small trailing model.

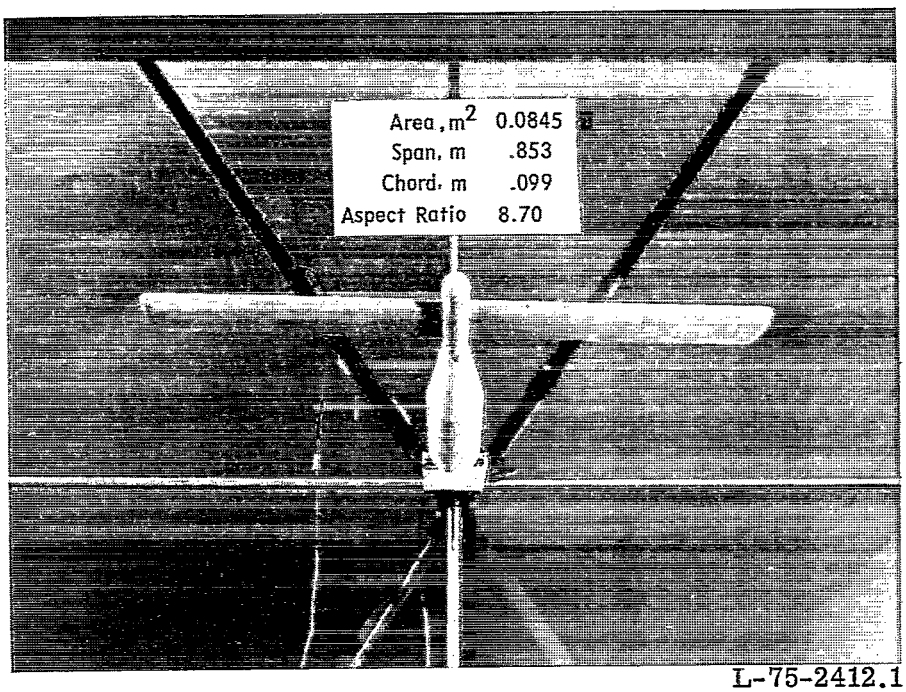

L-75-2412.1

(b) Large trailing model.

Figure 6.- Photographs of unswept trailing wing models on traverse mechanism. Both models have NACA 0012 airfoil sections.

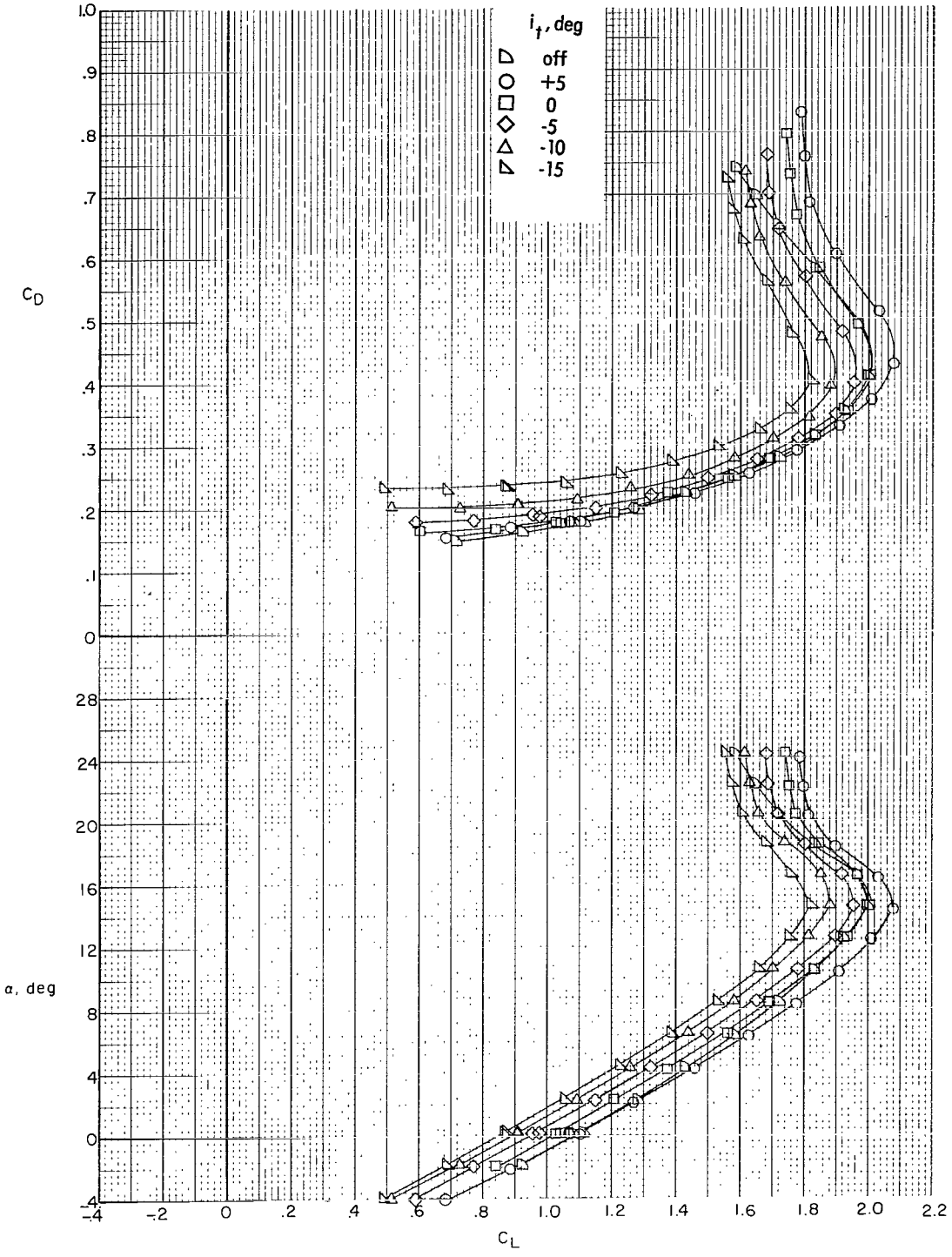

(a) Lift and drag coefficients.

Figure 7.- Effect of horizontal-tail incidence on longitudinal aerodynamic characteristics of transport aircraft model; $\delta_{f,i} = 30^o$; $\delta_{f,o} = 30^o$.

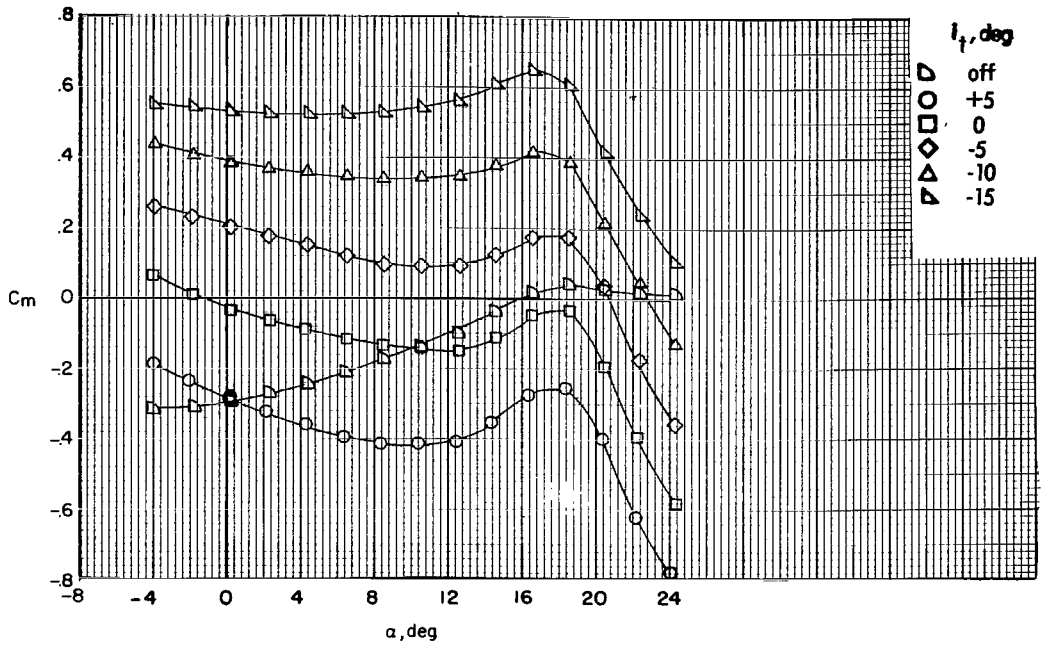

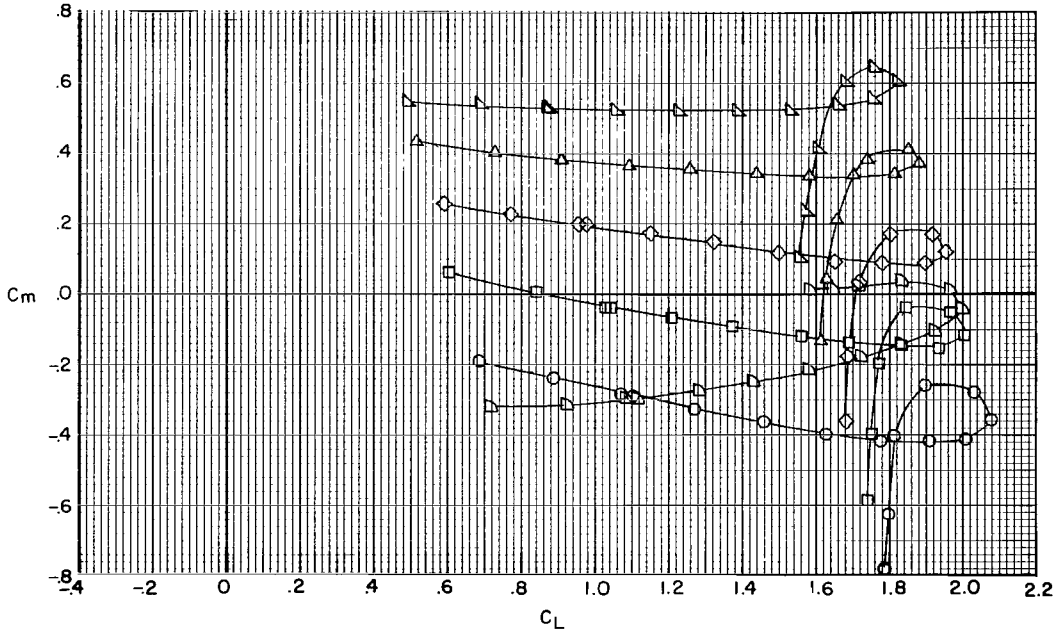

(b) Pitching-moment coefficient.

Figure 7.- Concluded.

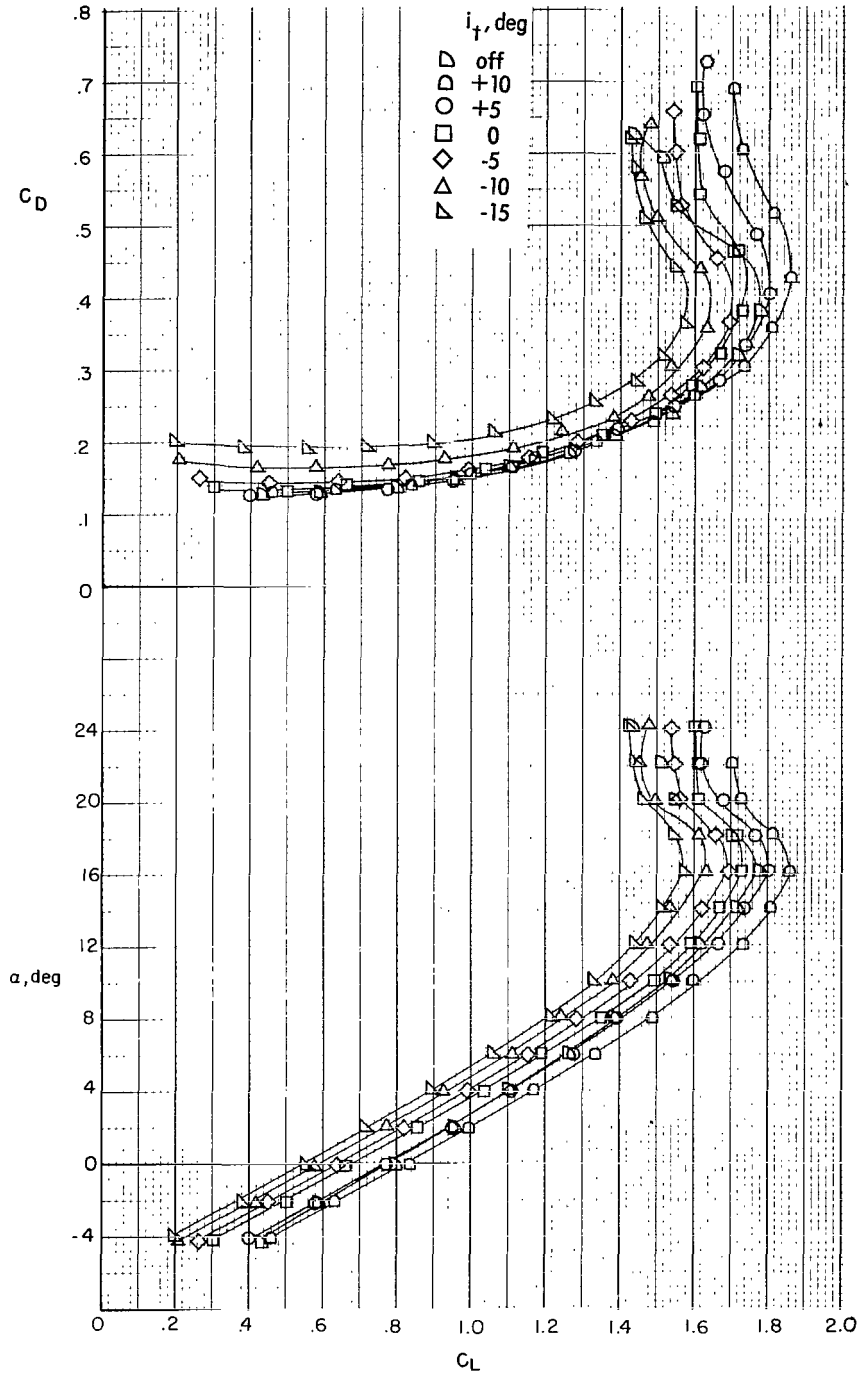

(a) Lift and drag coefficients.

Figure 8.- Effect of horizontal-tail incidence on longitudinal aerodynamic characteristics of transport aircraft model; $\delta_{f,i} = 30^{o}$; $\delta_{f,o} = 0^{o}$.

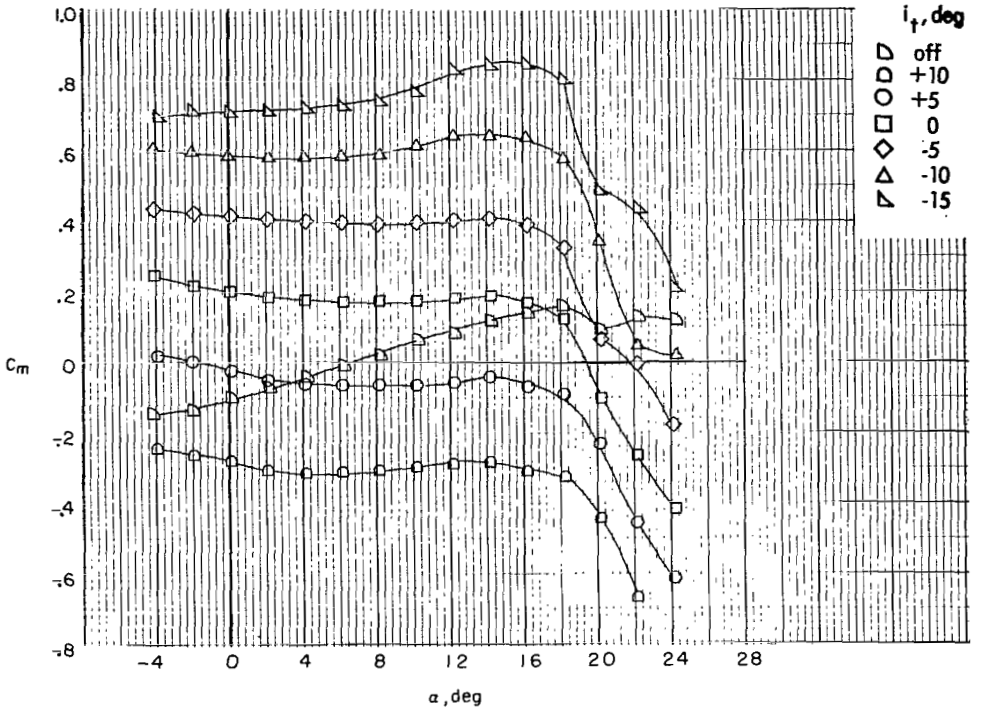

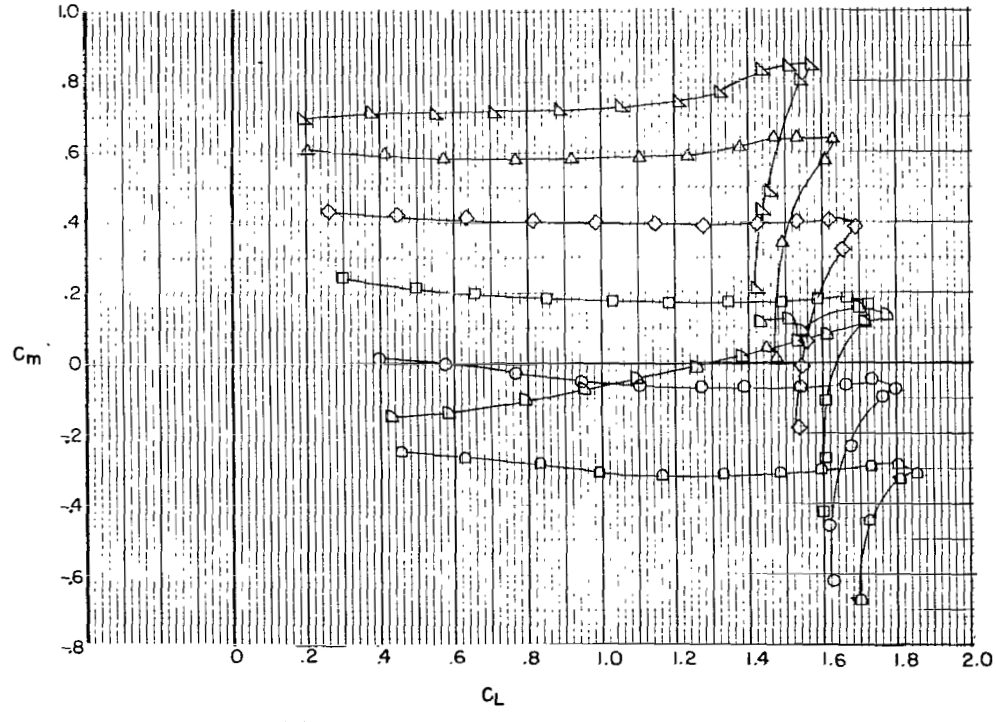

(b) Pitching-moment coefficient.

Figure 8.- Concluded.

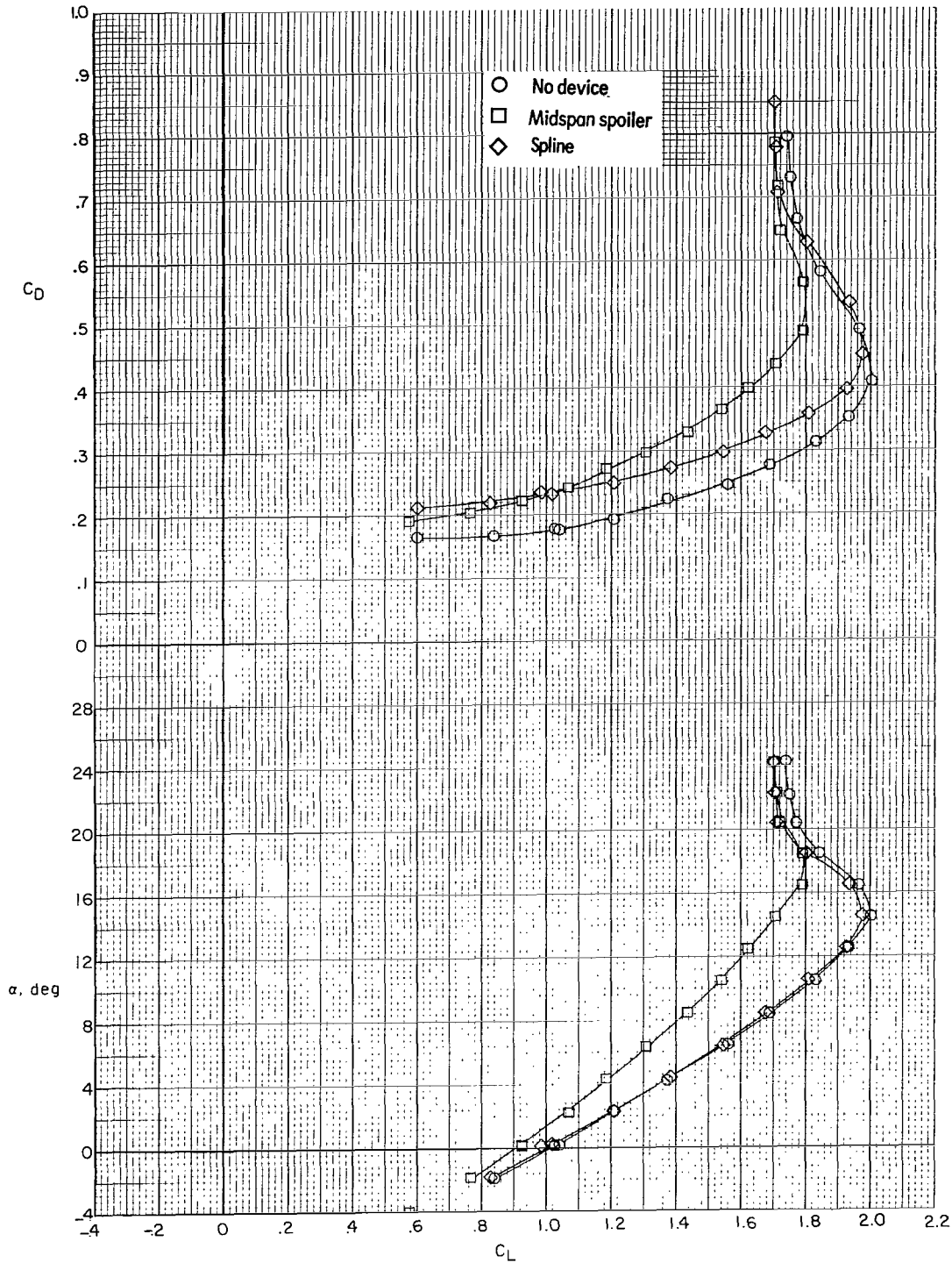

(a) Lift and drag coefficients.

Figure 9.- Effect of midspan spoiler and spline on longitudinal aerodynamic characteristics of transport aircraft model; $\delta_{f,i} = 30^o$; $\delta_{f,o} = 30^o$; $i_t = 0^o$.

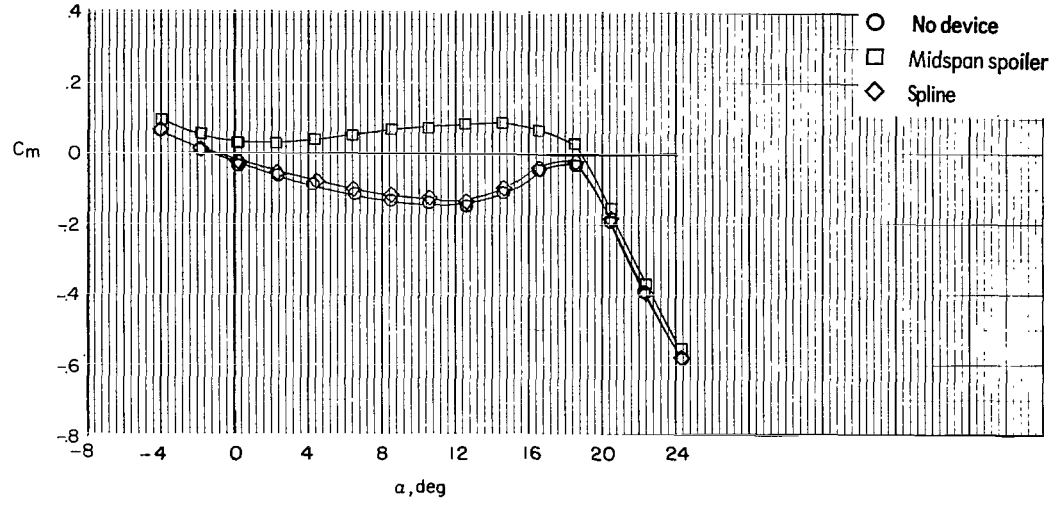

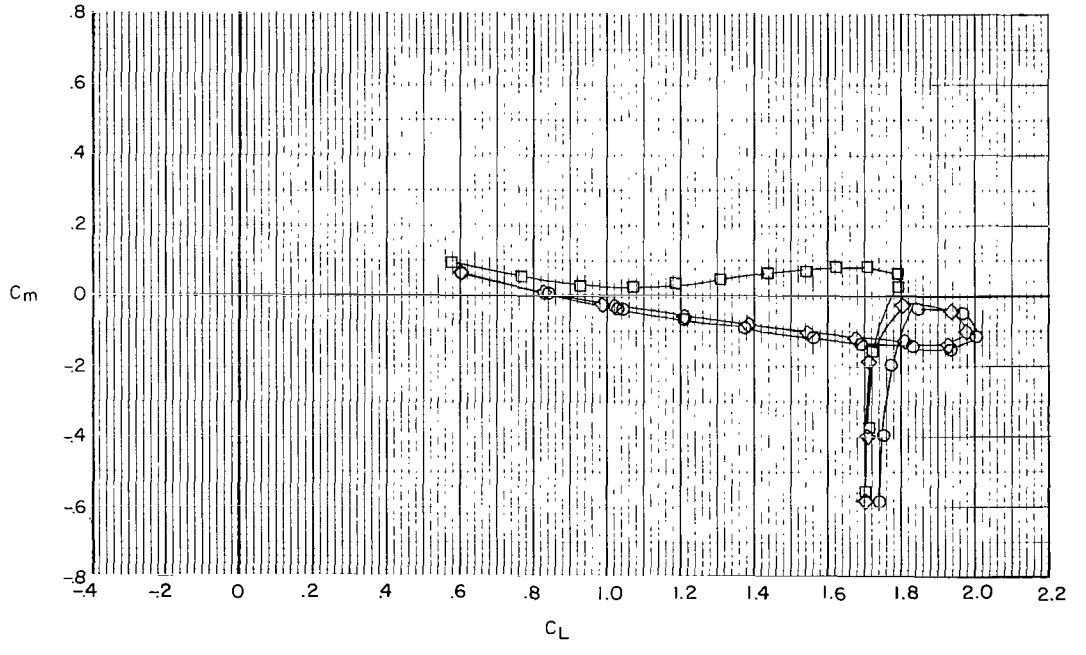

(b) Pitching-moment coefficient.

Figure 9.- Concluded.

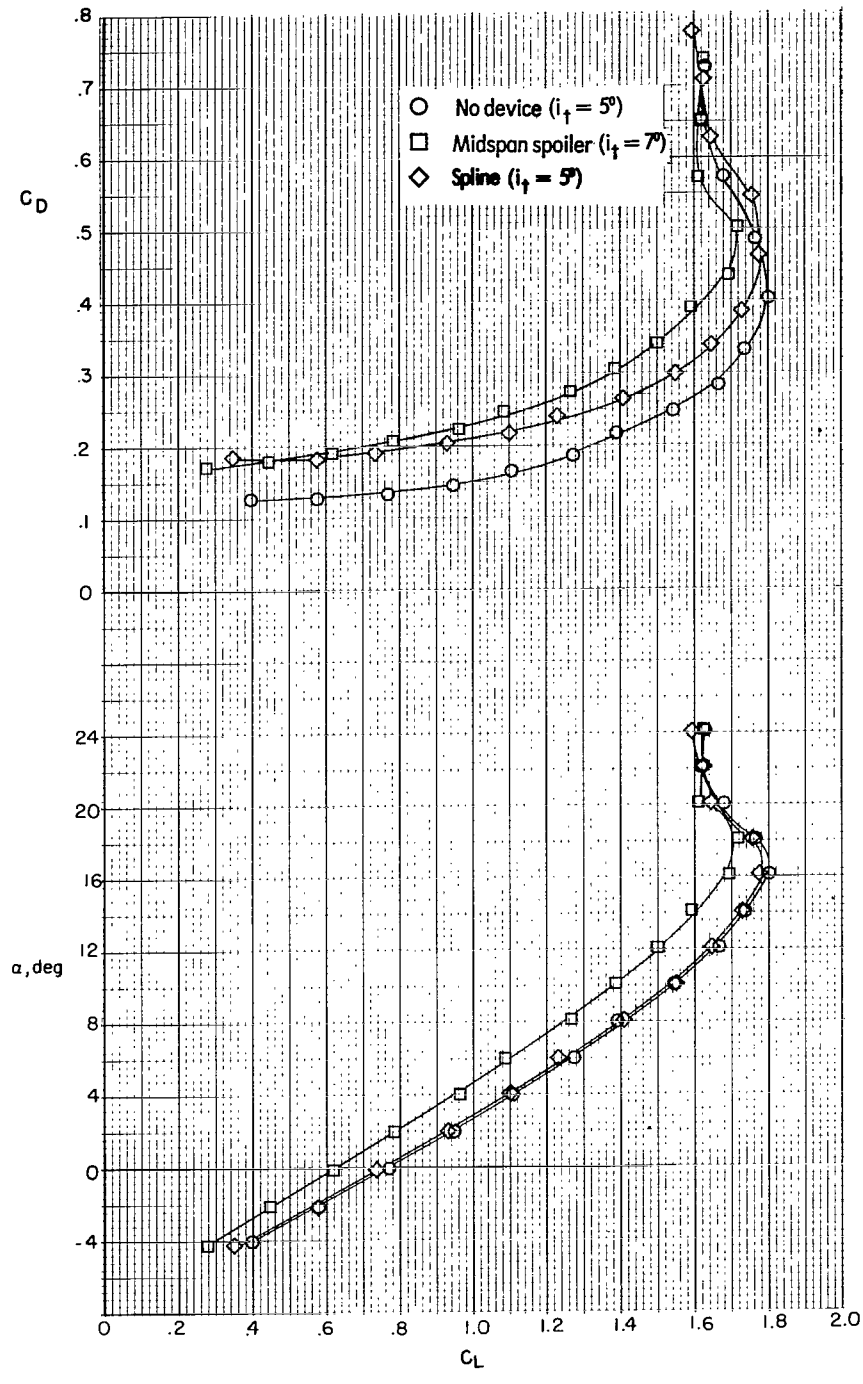

(a) Lift and drag coefficients.

Figure 10.- Effect of midspan spoiler and spline on longitudinal aerodynamic characteristics of transport aircraft model; $\delta_{f,i} = 30^{o}$; $\delta_{f,o} = 0^{o}$.

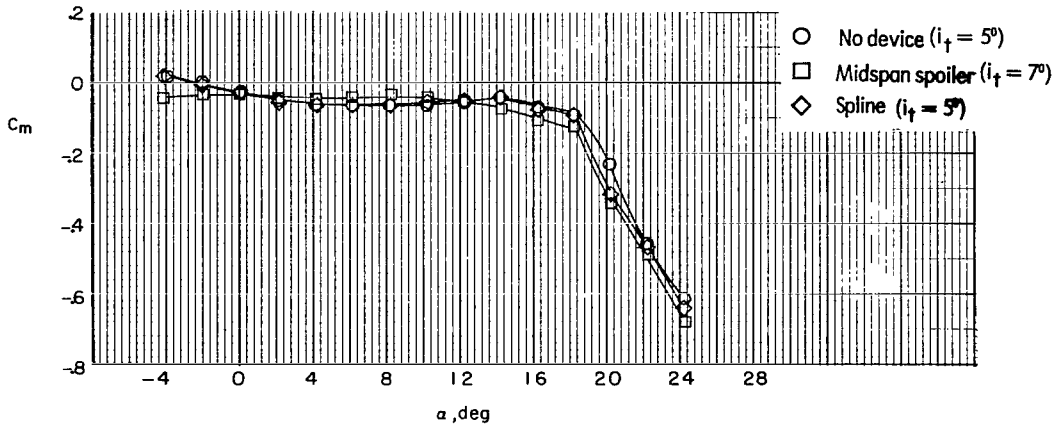

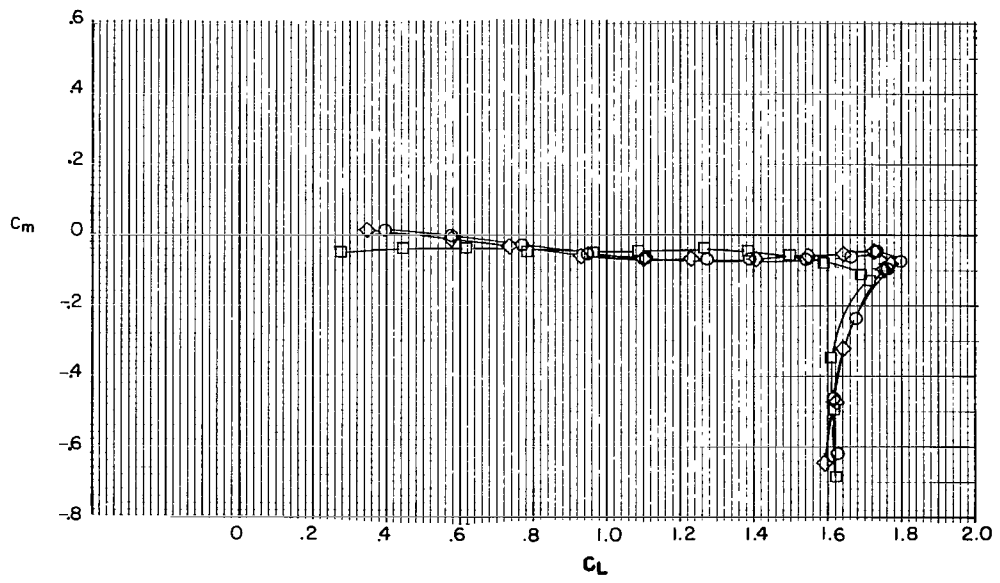

(b) Pitching-moment coefficient.

Figure 10.- Concluded.

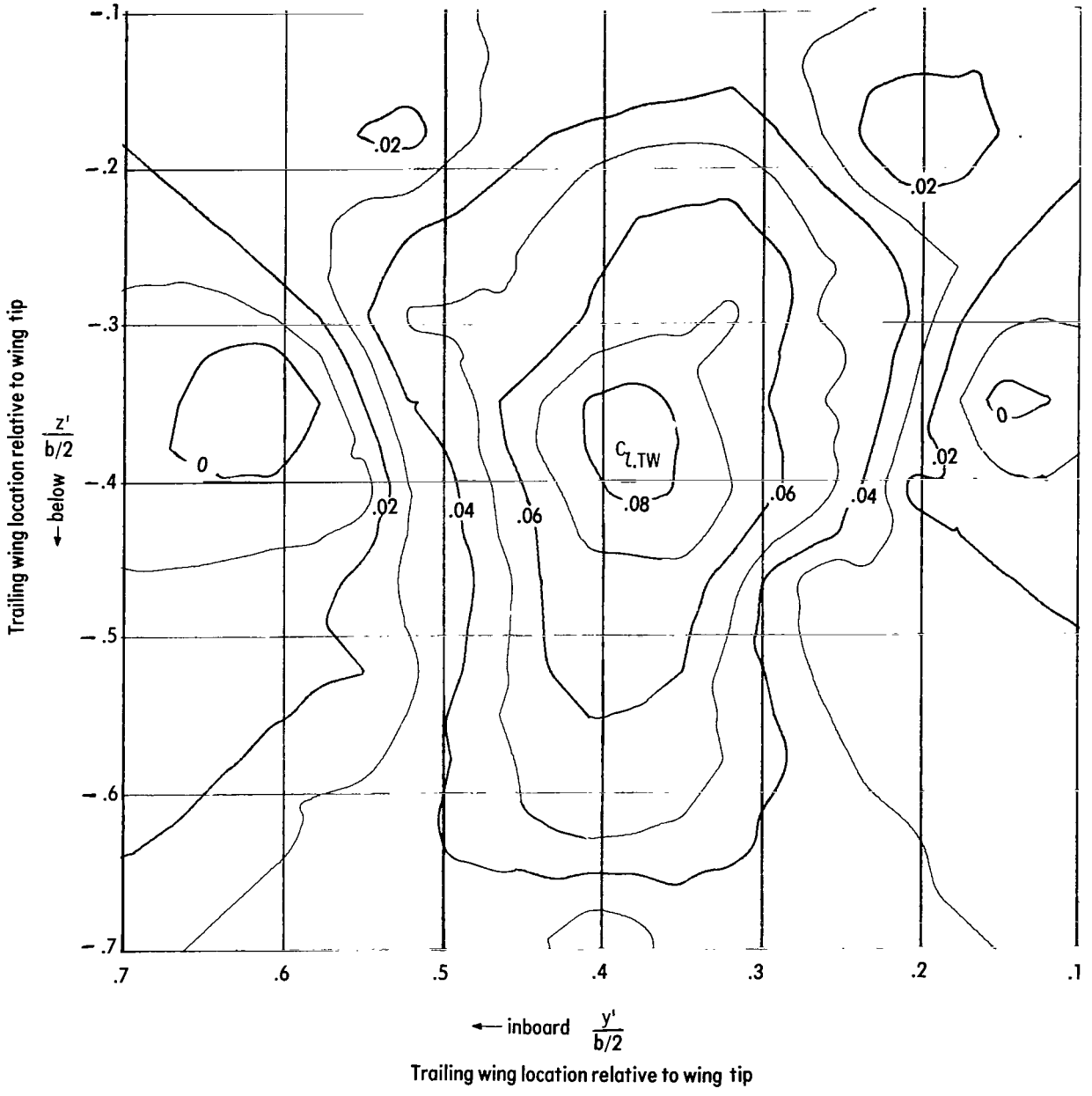

(a) Small trailing model.

Figure 11.- Contour plot of rolling-moment coefficients measured on trailing models at 6.74 spans downstream of transport aircraft model with flap configuration $30^o/30^o$. $C_L = 1.2$.

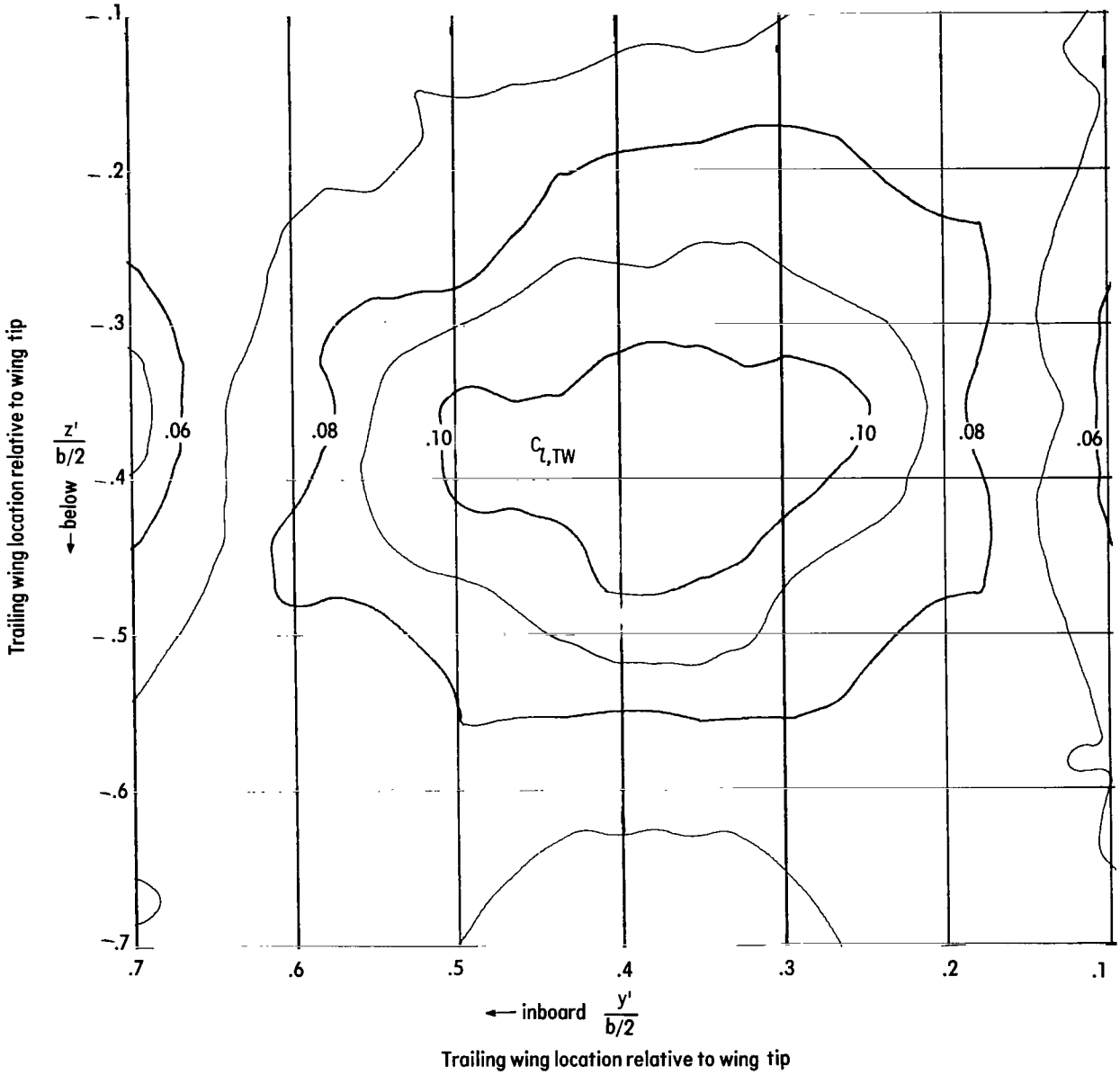

(b) Large trailing model.

Figure 11.- Concluded.

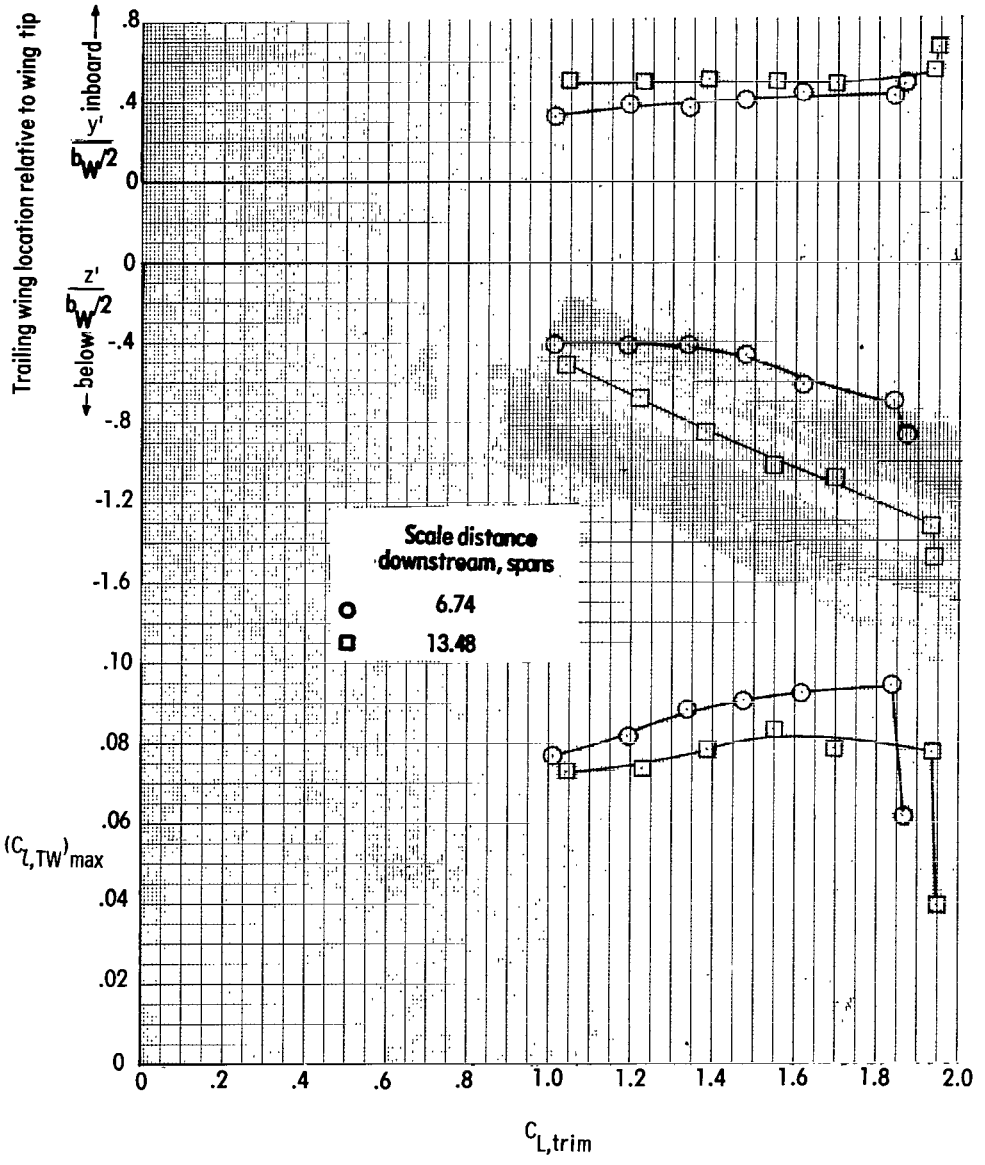

(a) Small trailing model.

Figure 12.- Variation of trailing model location and trailing wing rolling-moment coefficient with trim lift coefficient of transport aircraft model at 6.74 and 13.48 spans downstream of transport aircraft model; $\delta_{f,i} = 30^{o}$; $\delta_{f,o} = 30^{o}$; $C_m = 0$.

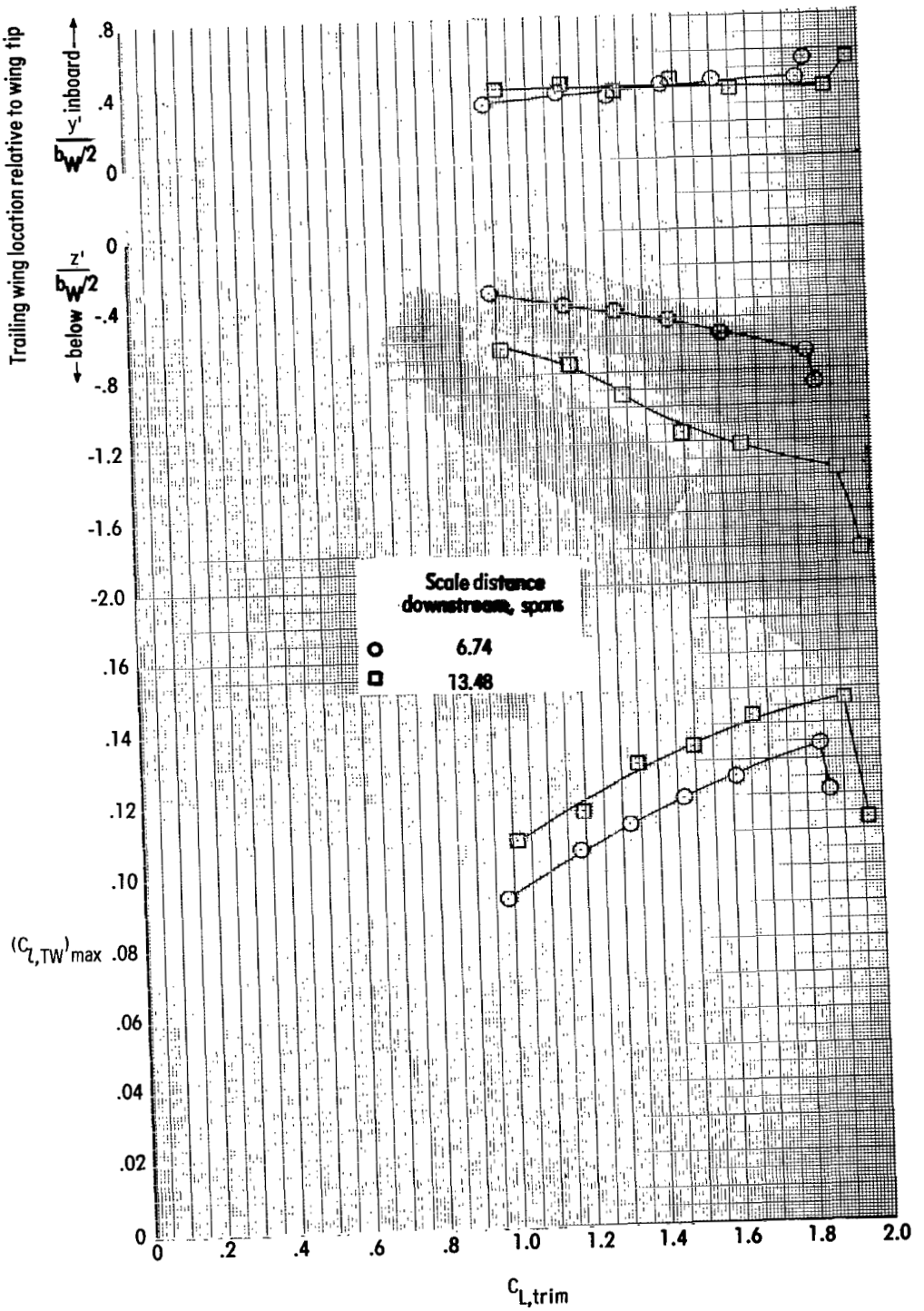

(b) Large trailing model.

Figure 12.- Concluded.

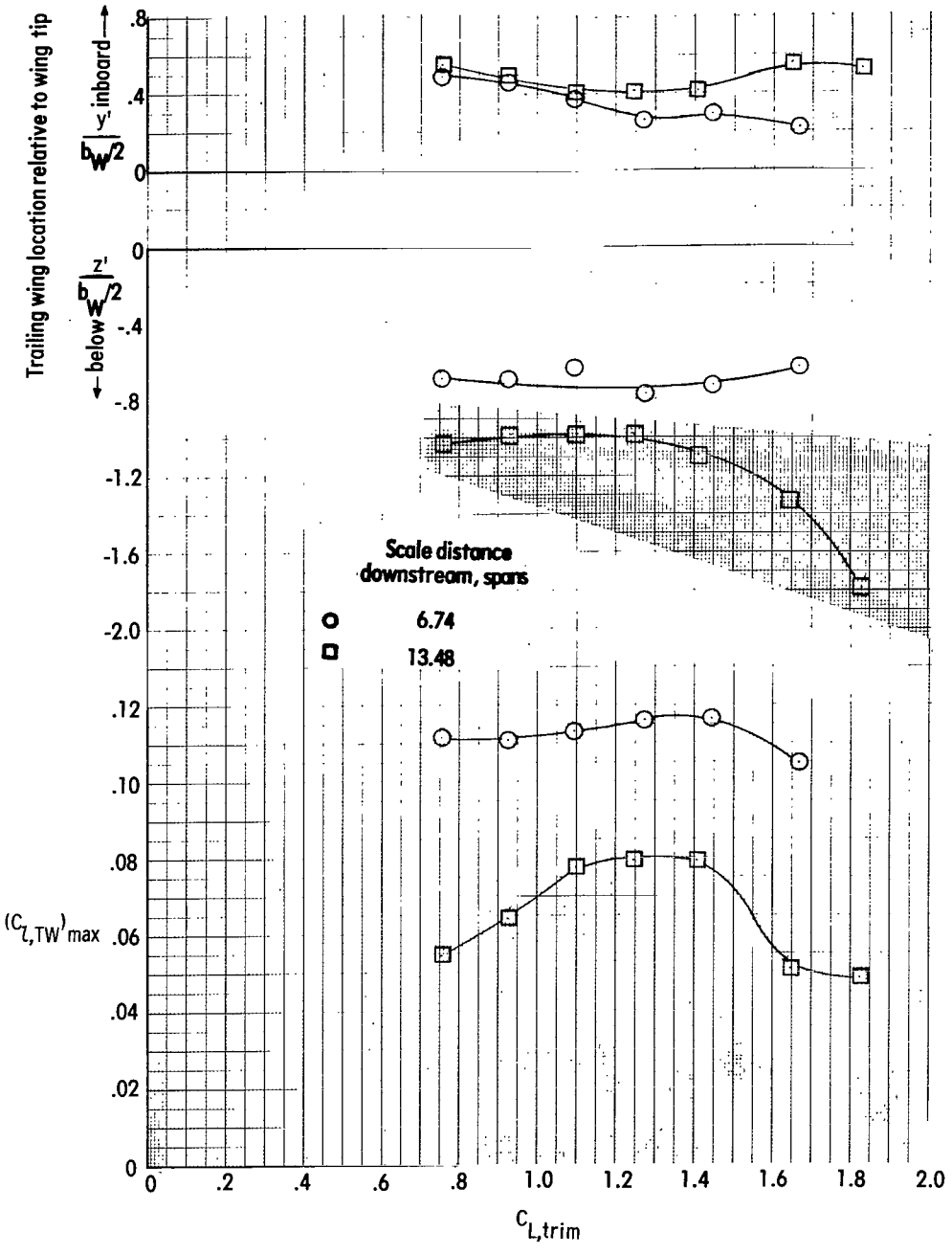

(a) Small trailing model.

Figure 13.- Variation of trailing model location and trailing wing rolling-moment coefficient with trim lift coefficient of transport aircraft model at 6.74 and 13.48 spans downstream of transport aircraft model; $\delta_{f,i} = 30^{o}$; $\delta_{f,o} = 0^{o}$; $C_m = 0$.

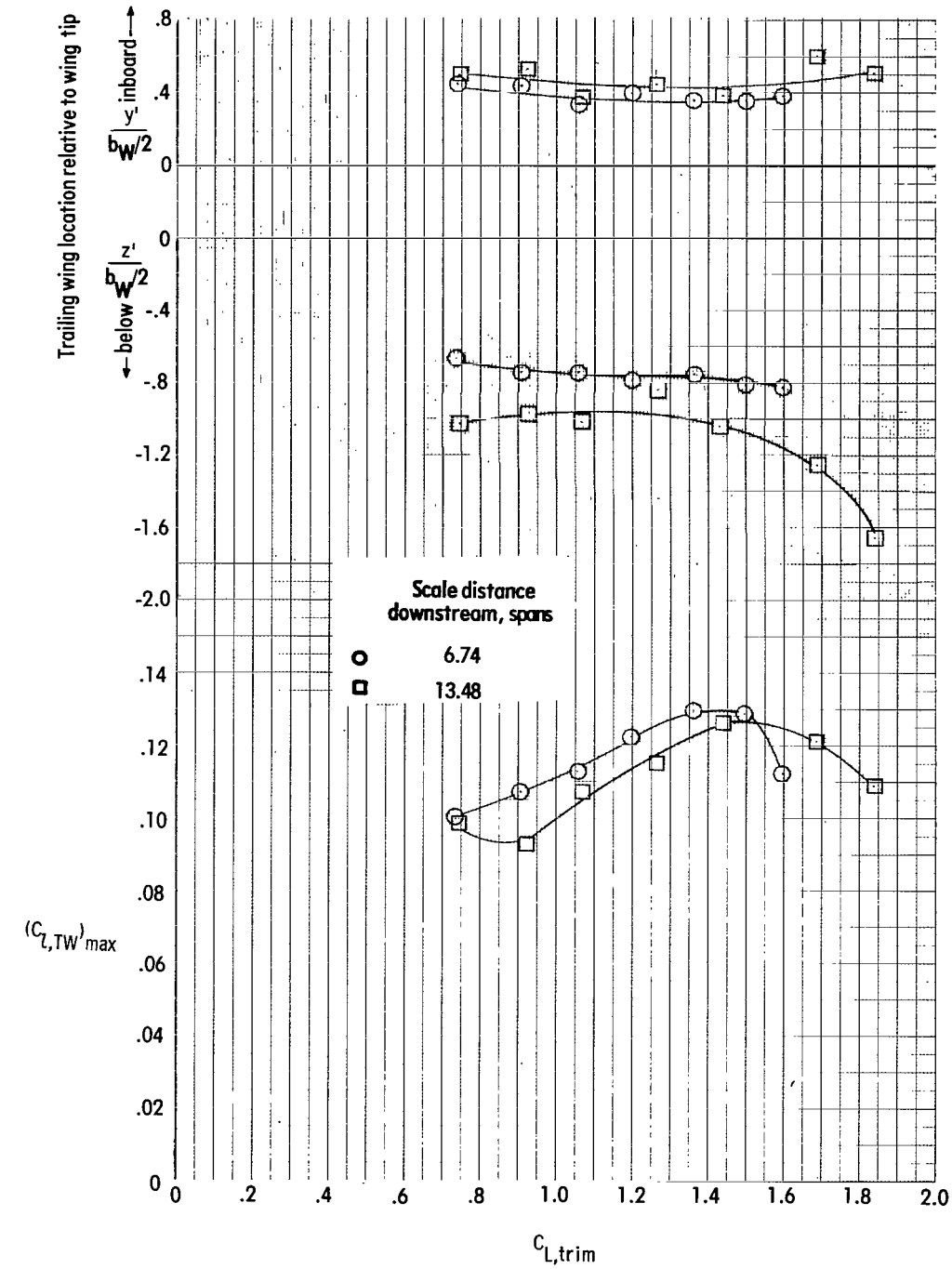

(b) Large trailing model.

Figure 13.- Concluded.

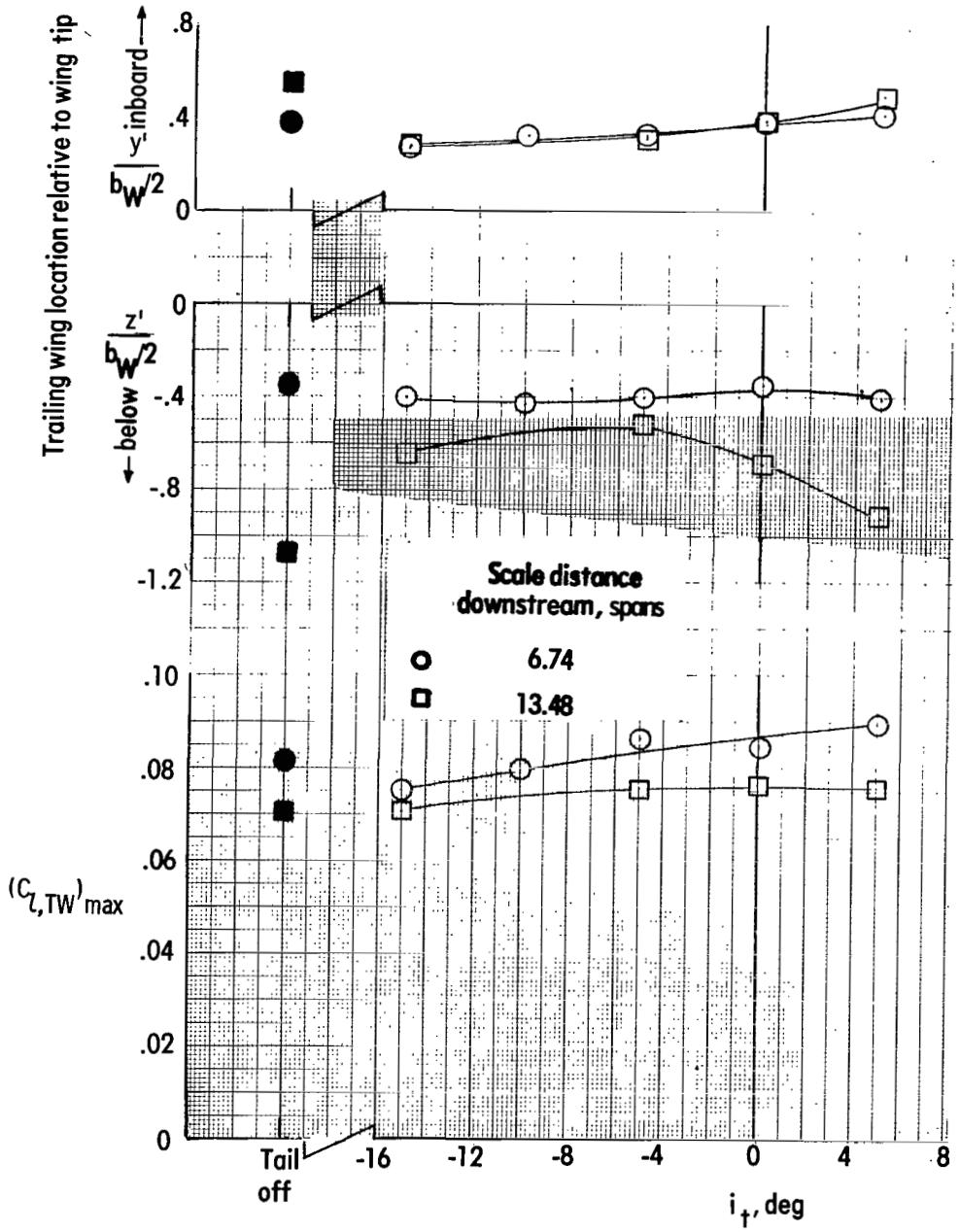

(a) Small trailing model.

Figure 14.- Variation of trailing model location and trailing wing rolling-moment coefficient with tail incidence of transport aircraft model at 6.74 and 13.48 spans downstream of transport aircraft model; $\delta_{f,i} = 30^{o}$; $\delta_{f,o} = 30^{o}$; $C_L = 1.2$.

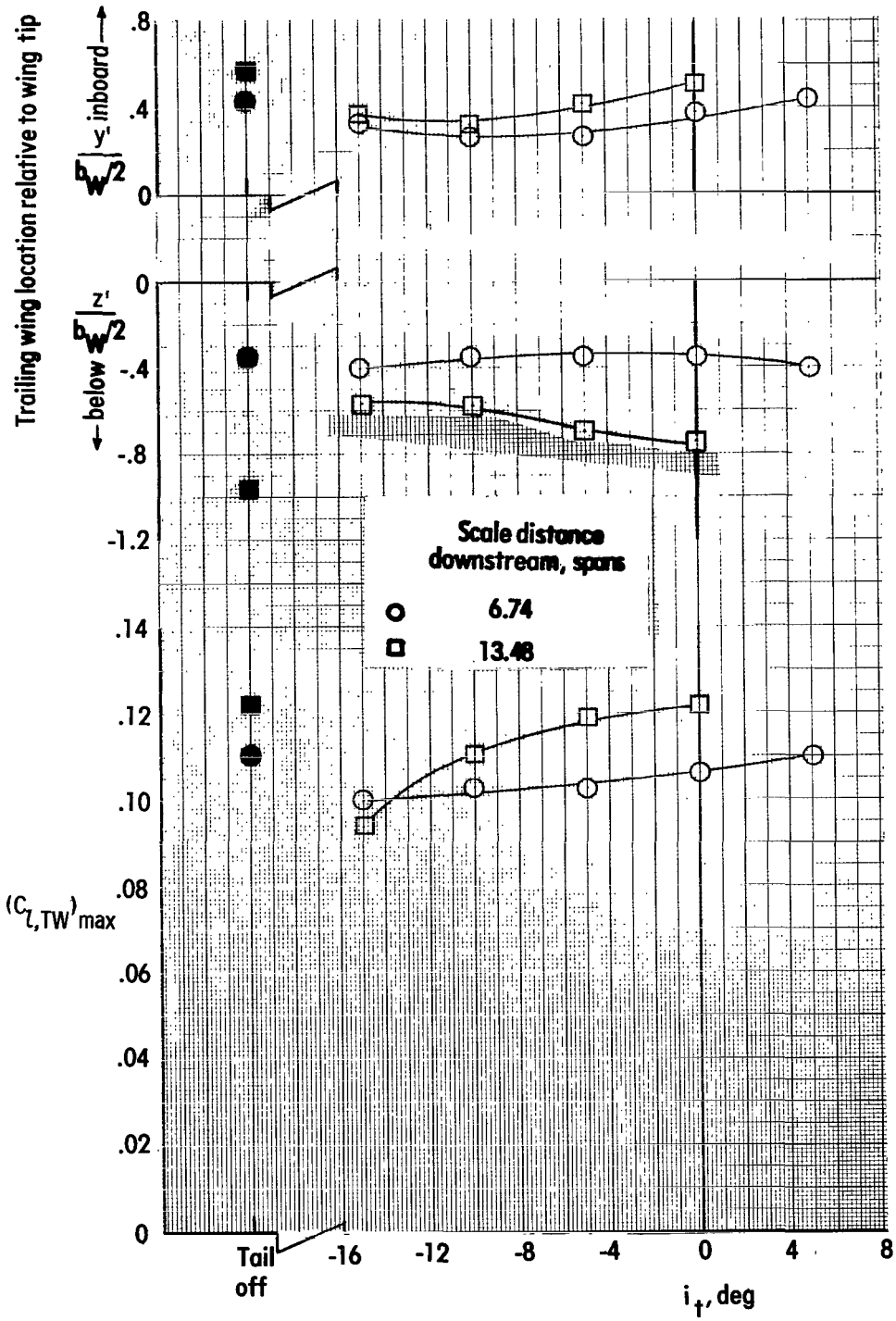

(b) Large trailing model.

Figure 14.- Concluded.

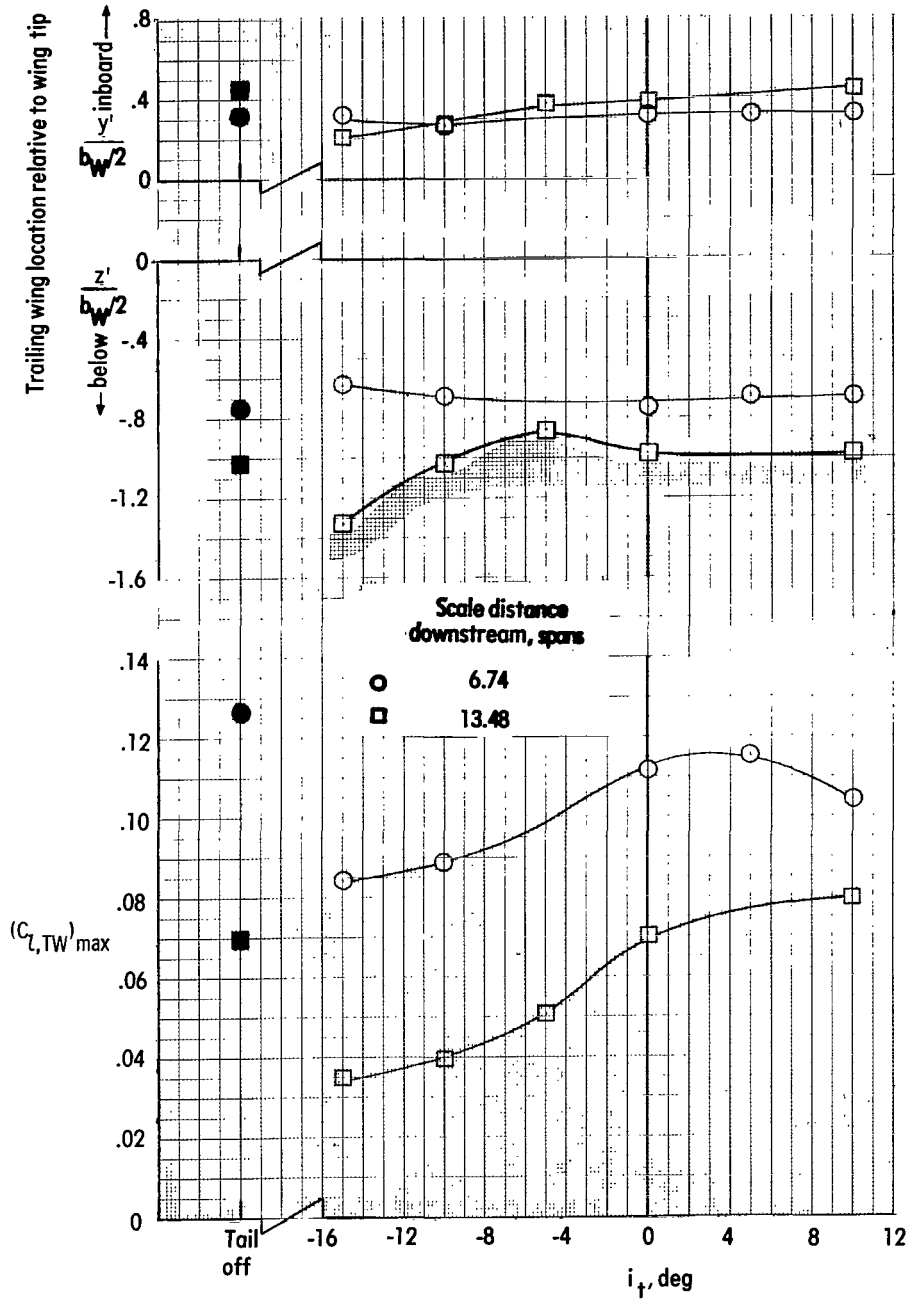

(a) Small trailing model.

Figure 15.- Variation of trailing model location and trailing wing rolling-moment coefficient with tail incidence of transport aircraft model at 6.74 and 13.48 spans downstream of transport aircraft model; $\delta_{f,i} = 30^o$; $\delta_{f,o} = 0^o$; $C_L = 1.2$.

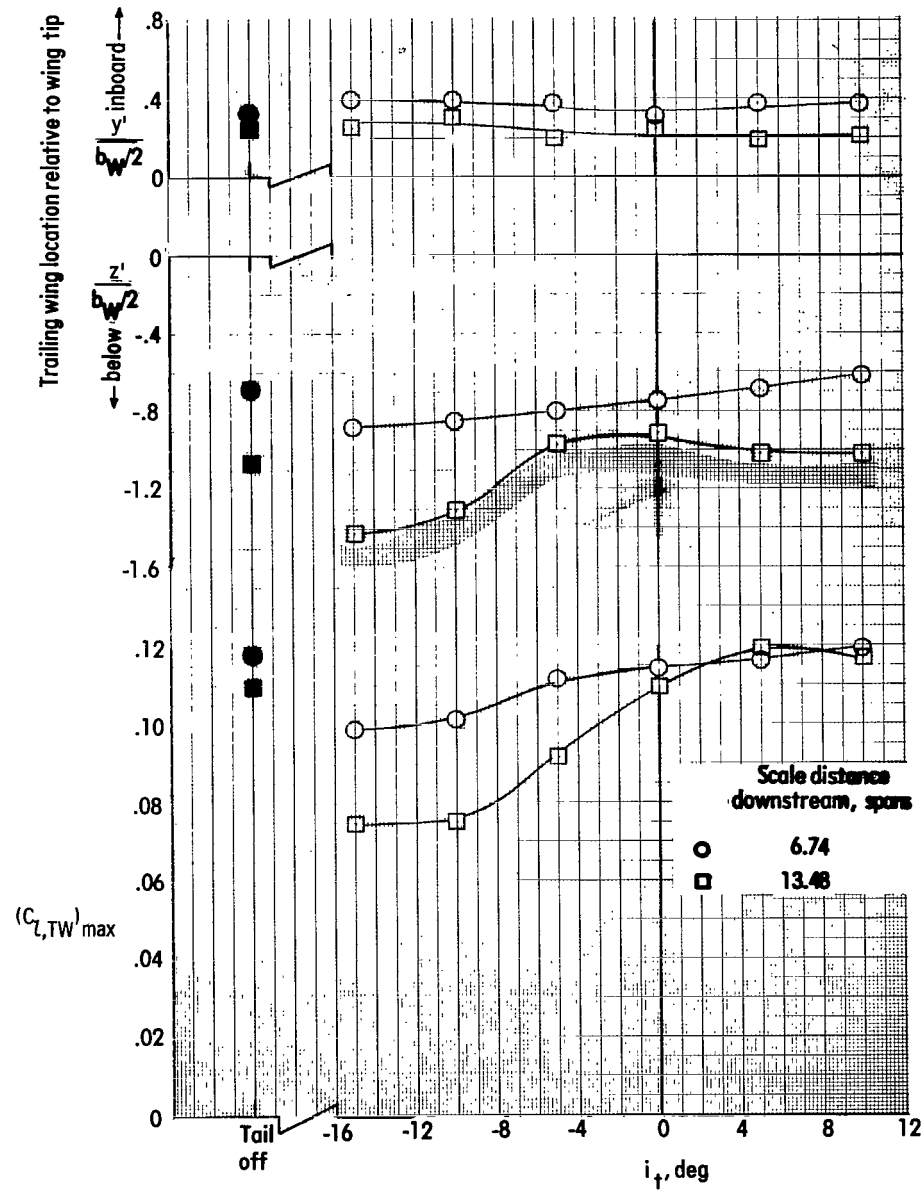

(b) Large trailing model.

Figure 15.- Concluded.

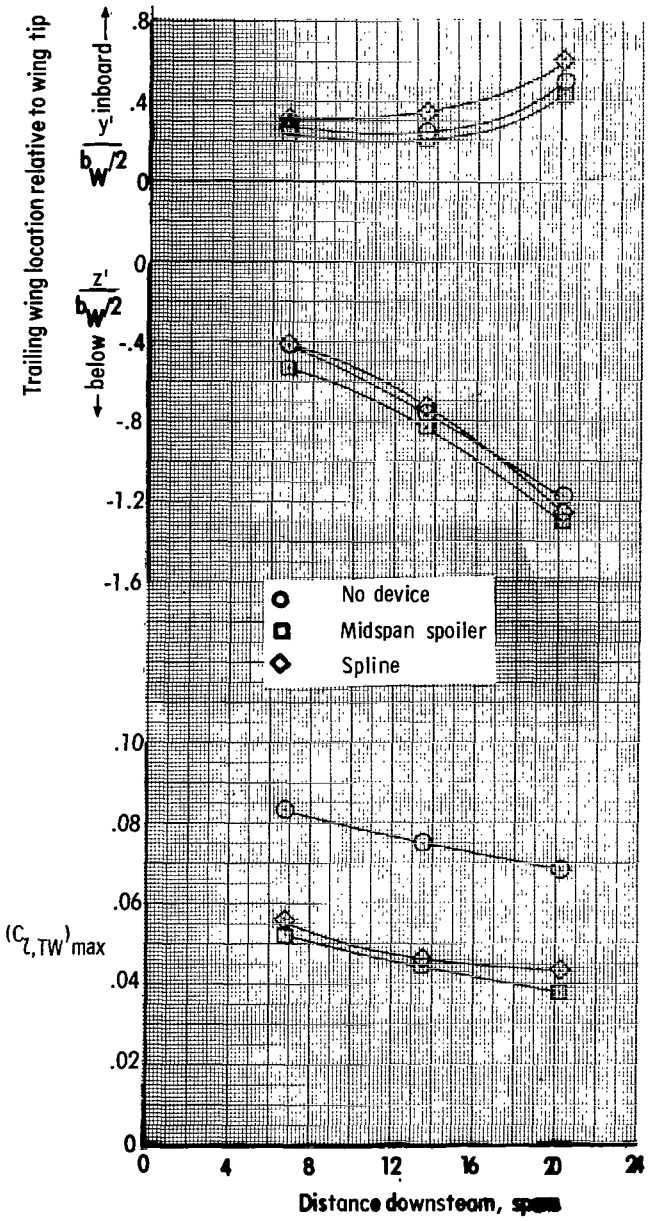

(a) Small trailing model.

Figure 16.- Variation of trailing model location and trailing wing rolling-moment coefficient with distance downstream of transport aircraft model equipped with vortex-attenuation devices; $\delta_{f,i} = 30^{o}$; $\delta_{f,o} = 30^{o}$; $C_{L,trim} = 1.2$.

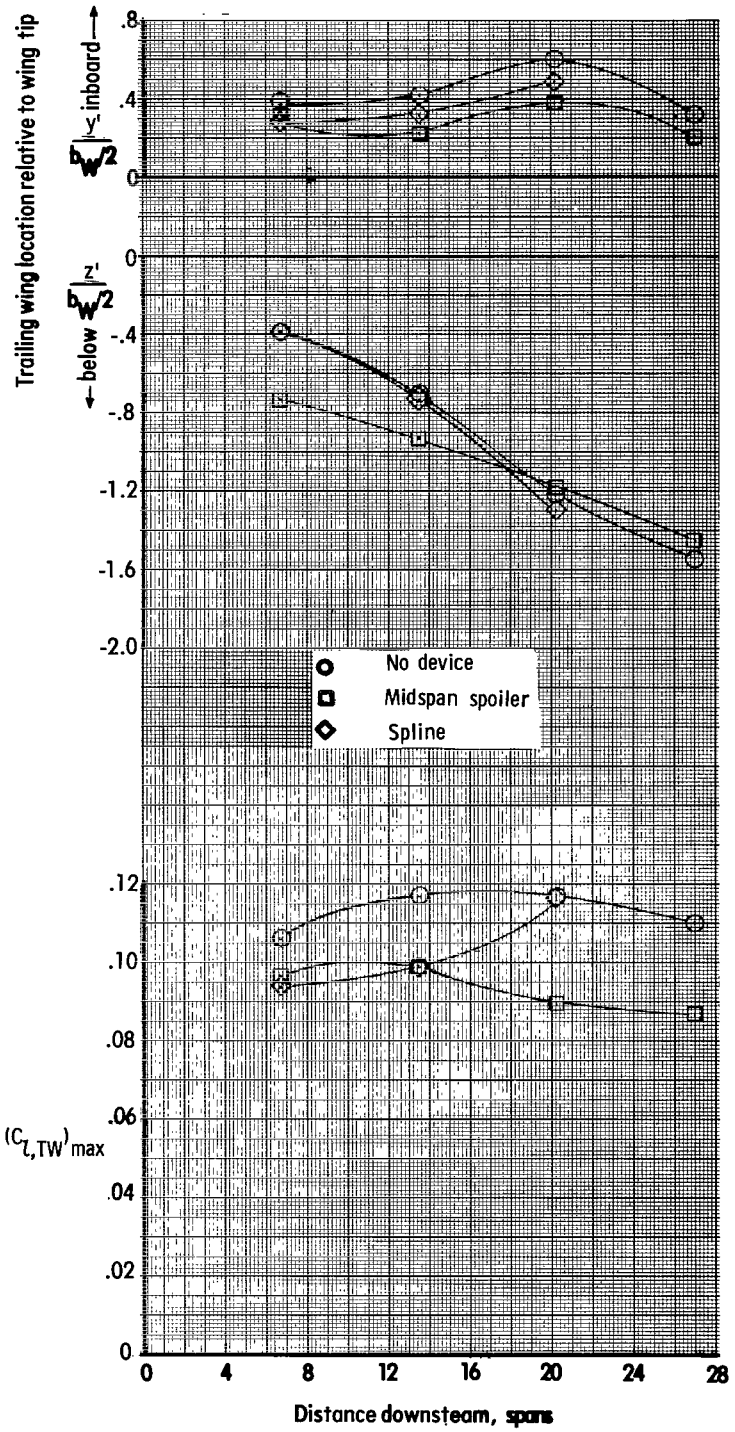

(b) Large trailing model.

Figure 16.- Concluded.

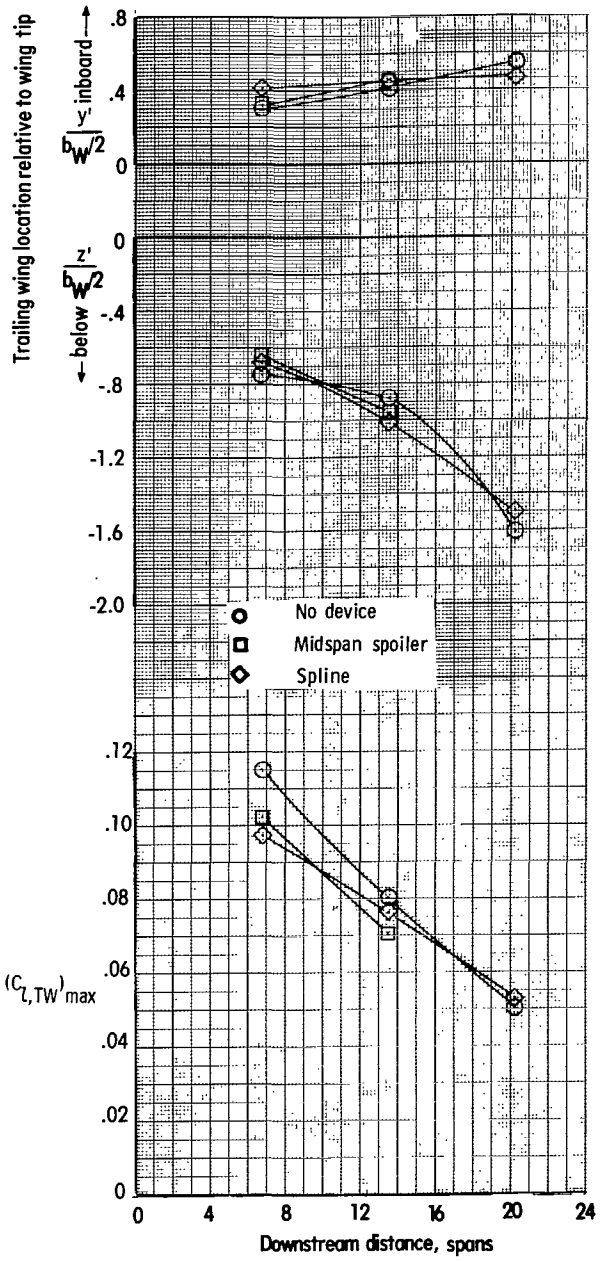

(a) Small trailing model.

Figure 17.- Variation of trailing model location and trailing wing rolling-moment coefficient with distance downstream of transport aircraft model equipped with vortex-attenuation devices; $\delta_{f,i} = 30^o$; $\delta_{f,o} = 0^o$; $C_{L,trim} = 1.2$.

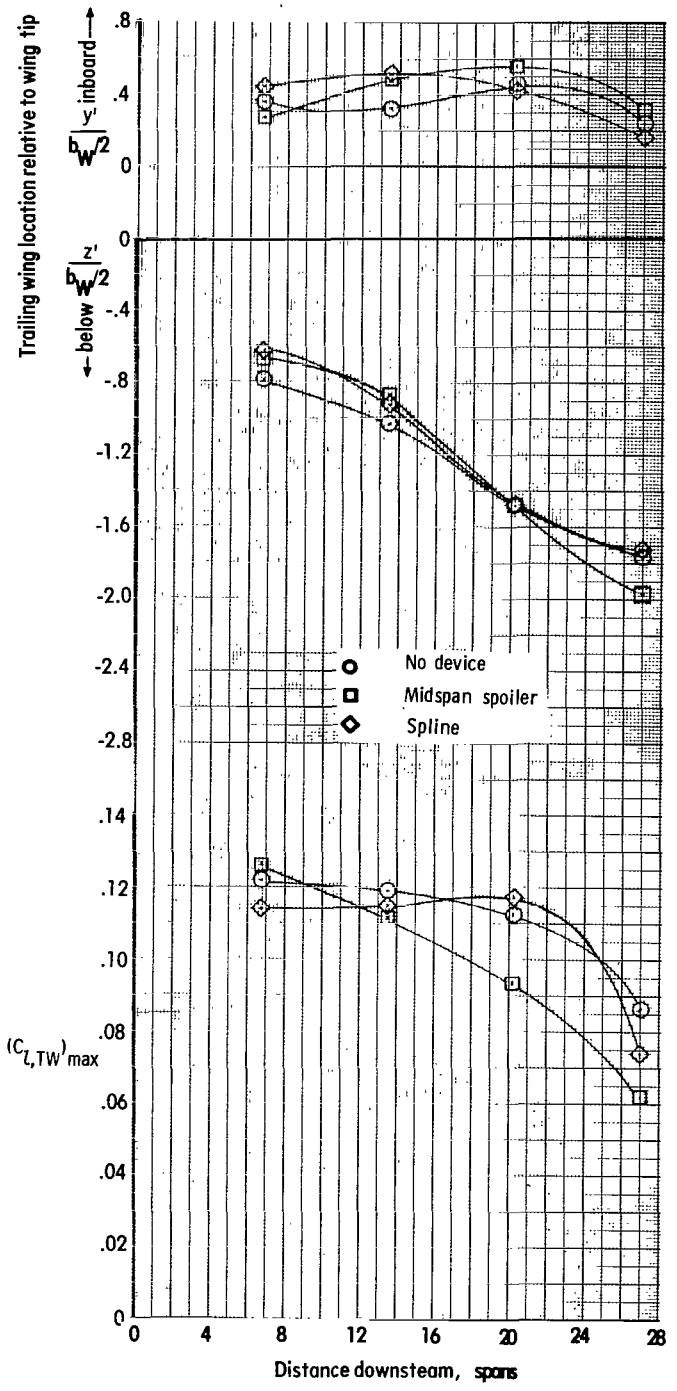

(b) Large trailing model.

Figure 17.- Concluded.

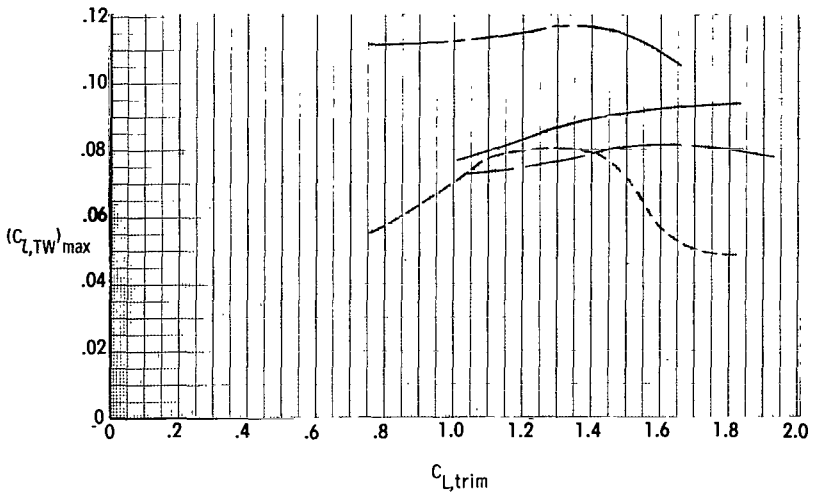

(a) Small trailing model.

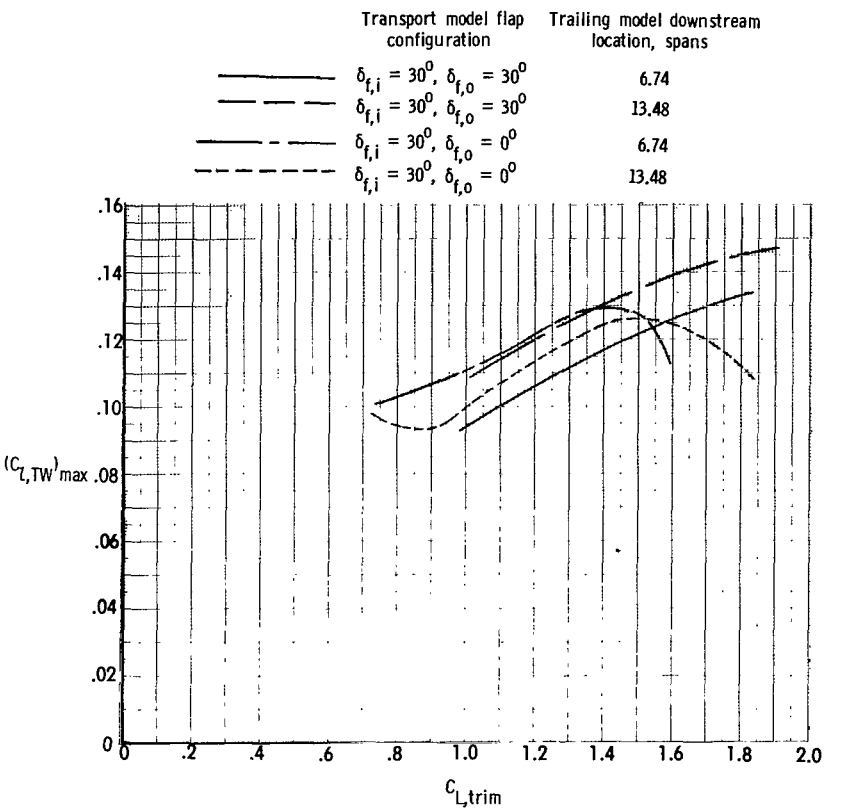

(b) Large trailing model.

Figure 18.- Variation of trailing wing rolling-moment coefficient with transport aircraft model lift coefficient at 6.74 and 13.48 spans downstream of transport aircraft model. $C_m = 0$.

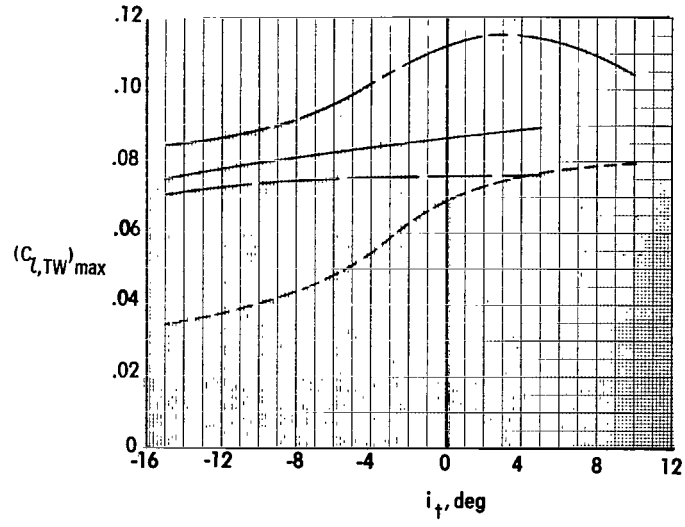

(a) Small trailing model.

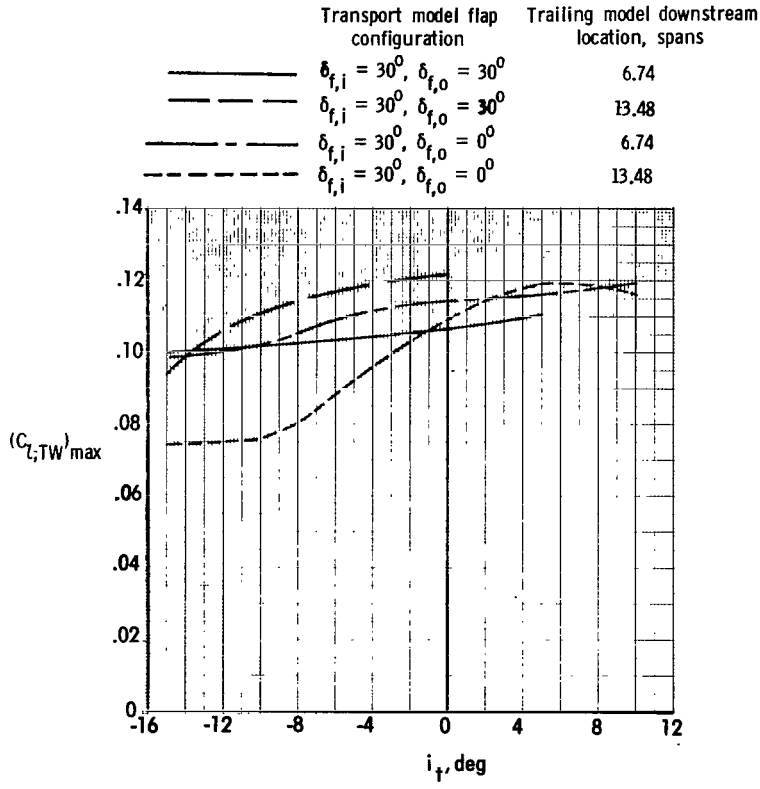

(b) Large trailing model.

Figure 19.- Variation of trailing wing rolling-moment coefficient with transport aircraft model horizontal-tail incidence at 6.74 and 13.48 spans downstream of transport aircraft model. $C_L = 1.2$.

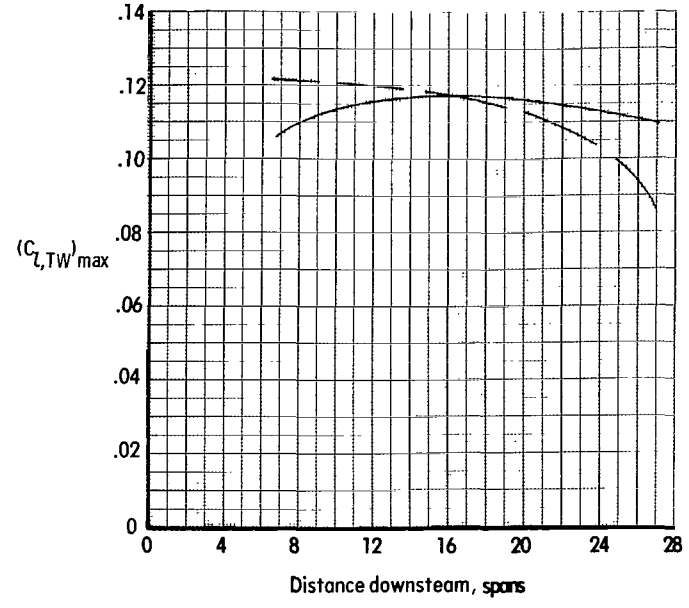

(a) Large trailing model.

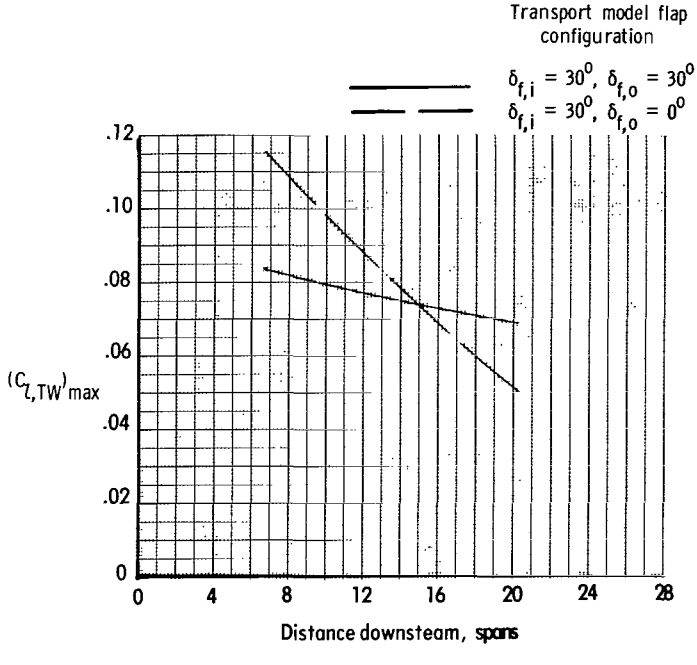

(b) Small trailing model.

Figure 20.- Variation of trailing wing rolling-moment coefficient with distance downstream of transport aircraft model. $C_{L,trim} = 1.2$.

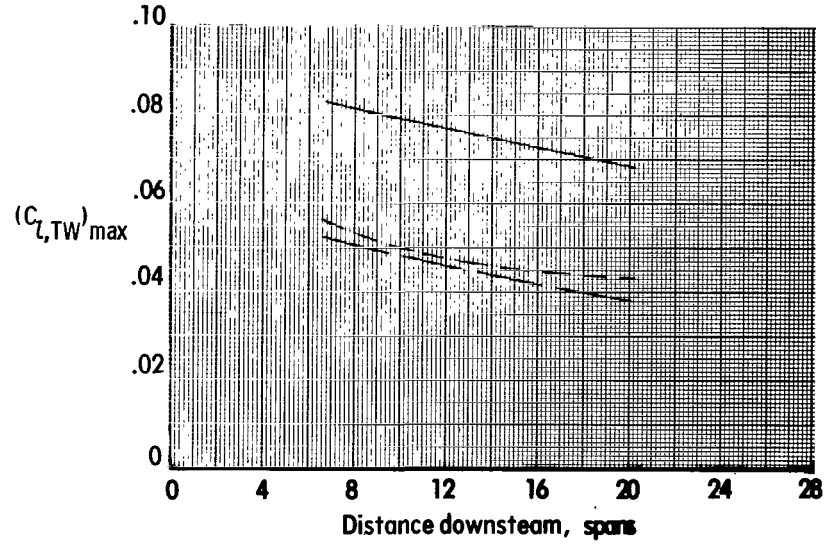

(a) Transport aircraft model with $\delta_{f,i} = 30^{o}$ and $\delta_{f,o} = 30^{o}$ and small trailing model.

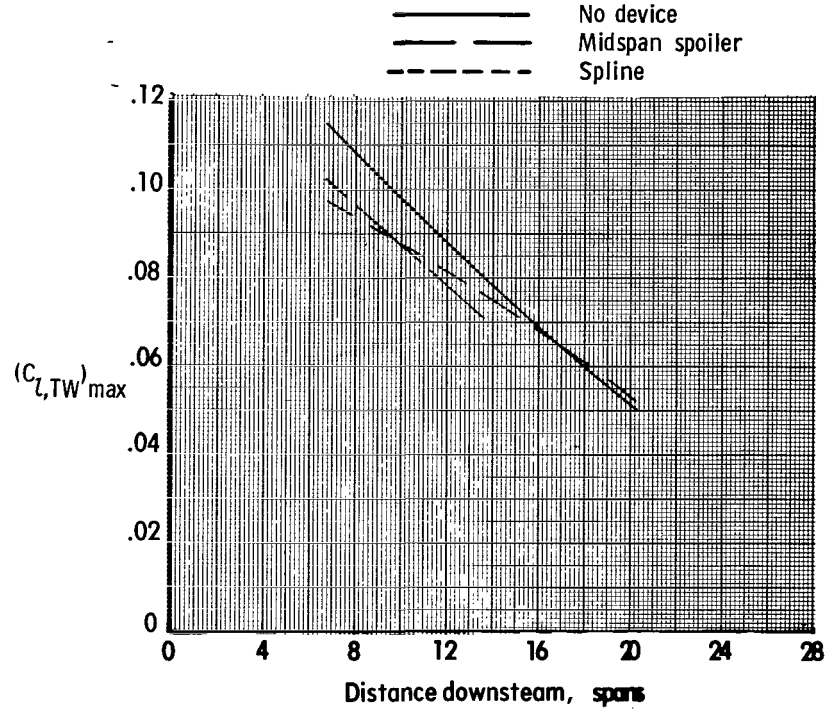

(b) Transport aircraft model with $\delta_{f,i} = 30^{o}$ and $\delta_{f,o} = 0^{o}$ and small trailing model.

Figure 21.- Variation of trailing wing rolling-moment coefficient with distance downstream of transport aircraft model with spoilers and transport aircraft model with splines. $C_{L,trim} = 1.2$.

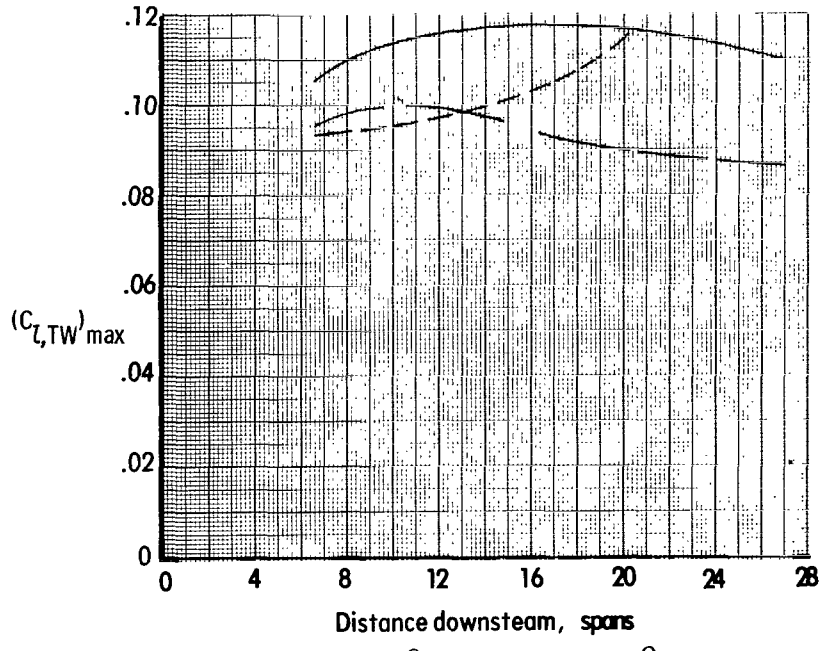

(c) Transport aircraft model with $\delta_{f,i} = 30^{o}$ and $\delta_{f,o} = 30^{o}$ and large trailing model.

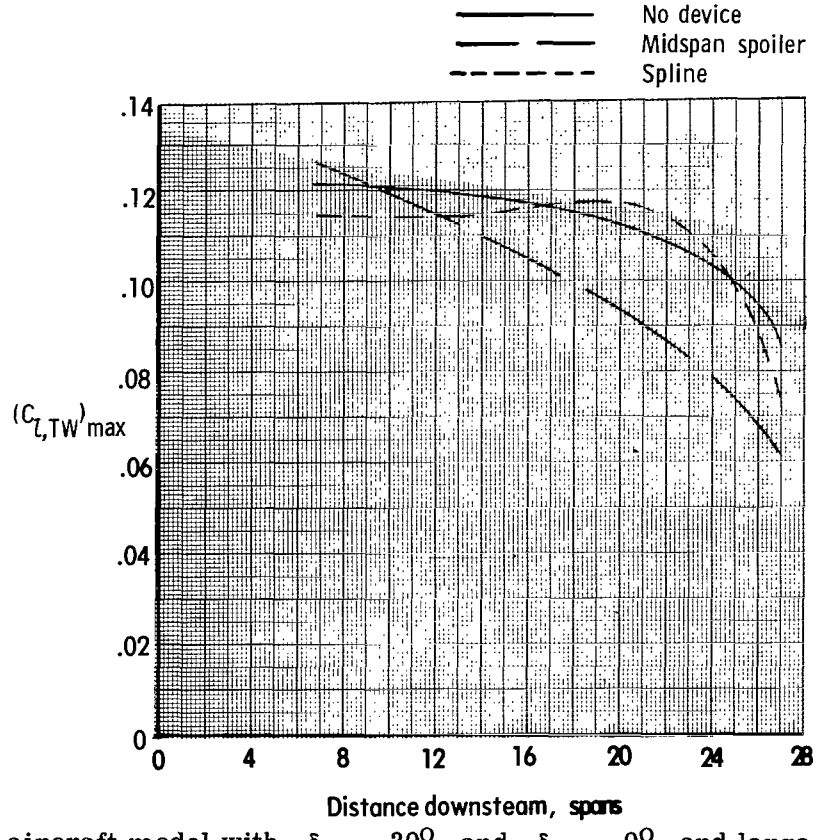

(d) Transport aircraft model with $\delta_{f,i} = 30^{o}$ and $\delta_{f,o} = 0^{o}$ and large trailing model.

Figure 21.- Concluded.